The Fine-Scale Magnetic History of the Allende Meteorite: Implications for the Structure of the Solar Nebula

Roger Fu, Michael Volk, Dario Bilardello, Guy Libourel, Geoffroy Lesur, Oren Ben Dor

AGU Advances

RESEARCH ARTICLE
10.1029/2021AV000486

This article is a companion to Nichols (2021), https://doi.org/10.1029/2021AV000511.

Key Points:

- Strong magnetization in Allende is carried by only a single ferromagnetic mineral-pyrrhotite-while other minerals are weakly magnetized
- This peculiar pattern of magnetization is best explained by acquisition during aqueous alteration in a strong nebular magnetic field
- The resulting paleointensity, >40 μT, suggests strong magnetic control on nebular accretion and heterogeneous conditions in the outer disk

Supporting Information:

Supporting Information may be found in the online version of this article.

Correspondence to:

R. R. Fu,
rogerfu@fas.harvard.edu

Citation:

Fu, R. R., Volk, M. W. R., Bilardello, D., Libourel, G., Lesur, G. R. J., & Ben Dor, O. (2021). The fine-scale magnetic history of the Allende meteorite: Implications for the structure of the solar nebula. *AGU Advances*, *2*, e2021AV000486. https://doi.org/10.1029/2021AV000486

Received 12 MAY 2021
Accepted 16 JUN 2021

Peer Review The peer review history for this article is available as a PDF in the Supporting Information.

Author Contributions:

Formal analysis: Roger R. Fu, Michael W. R. Volk, Guy Libourel, Geoffroy R. J. Lesur

The Fine-Scale Magnetic History of the Allende Meteorite: Implications for the Structure of the Solar Nebula

Roger R. Fu[1], Michael W. R. Volk[1], Dario Bilardello[2], Guy Libourel[3,4], Geoffroy R. J. Lesur[5], and Oren Ben Dor[1,6]

[1]Department of Earth and Planetary Sciences, Harvard University, Cambridge, MA, USA, [2]Department of Earth and Environmental Sciences, University of Minnesota, Minneapolis, MN, USA, [3]CNRS, Observatoire de la Côte d'Azur, Université Côte d'Azur, Lagrange, Nice, France, [4]Hawai'i Institute of Geophysics and Planetology, University of Hawai'i at Manoa, Honolulu, HI, USA, [5]CNRS, IPAG, Universite Grenoble Alpes, Grenoble, France, [6]Department of Physics, Harvard University, Cambridge, MA, USA

Abstract Magnetic fields in the early solar system may have driven the inward accretion of the protoplanetary disk (PPD) and generated instabilities that led to the formation of planets and ring and gap structures. The Allende carbonaceous chondrite meteorite records a strong early solar system magnetic field that has been interpreted to have a PPD, dynamo, or impact-generated origin. Using high-resolution magnetic field imaging to isolate the magnetization of individual grain assemblages, we find that only Fe-sulfides carry a coherent magnetization. Combined with rock magnetic analyses, we conclude that Allende carries a magnetization acquired during parent body chemical alteration at ~3.0–4.2 My after calcium aluminum-rich inclusions in an >40 μT magnetic field. This early age strongly favors a magnetic field of nebular origin instead of dynamo or solar wind alternatives. When compared to other paleomagnetic data from meteorites, this strong intensity supports a central role for magnetic instabilities in disk accretion and the presence of temporal variations or spatial heterogeneities in the disk, such as ring and gap structures.

Plain Language Summary The presence of magnetic fields during the formation stage of the solar system may have been critical for planet formation. One way to test this hypothesis is to observe both the strength and the degree of heterogeneity in early solar system magnetic fields; strong fields with significant local variations would suggest a key role for magnetic fields in governing the distribution of planet-forming materials. We performed both traditional paleomagnetic analyses and high-resolution magnetic field imaging experiments on the carbonaceous chondrite Allende. By identifying the sub-regions that carry a magnetization, we infer that the meteorite was magnetized during reactions between Fe-bearing minerals and aqueous fluids on the parent asteroid at 3.0–4.2 million years after solar system formation. These reactions occurred in an ambient magnetic field of at least 40 μT strength, which is much stronger than inferred from other meteorites of similar age. We therefore find evidence for strong, heterogeneous magnetic fields in the forming solar system, supporting the idea that magnetic fields mediated the concentration of solid materials, potentially leading to planet formation.

1. Introduction

Partially ionized gas in the planet-forming region of protoplanetary disks (PPDs) is theorized to have amplified and sustained magnetic fields (e.g., Bai, 2017; Béthune et al., 2017). The strength and morphology of these nebular magnetic fields hold far-reaching implications for mass and angular momentum transport, the radial distribution of mass, and the source of nebular turbulence, which may have been critical to planet formation (Johansen, 2009; Klahr et al., 2018; Riols & Lesur, 2019).

Paleomagnetic studies of meteorites and returned samples can, in principle, quantify the strength, orientation, and duration of magnetic fields in the PPD that formed the solar system, also called the solar nebula. However, because other potential sources of magnetic fields existed in the early solar system, the interpretation of meteorite paleomagnetism depends critically on correctly identifying the origin of magnetic fields recorded in a given sample.

Investigation: Roger R. Fu, Dario Bilardello
Methodology: Roger R. Fu, Michael W. R. Volk, Oren Ben Dor
Visualization: Roger R. Fu, Dario Bilardello
Writing – review & editing: Roger R. Fu, Michael W. R. Volk, Dario Bilardello, Guy Libourel, Geoffroy R. J. Lesur, Oren Ben Dor

Specifically, three non-nebular mechanisms have been proposed as sources of early solar system magnetic fields. Frequent high-velocity impacts, especially during giant planet migration, may have produced short-lived but strong magnetic fields on planetesimal surfaces, although such fields have been observed to-date only in laboratory settings (Crawford & Schultz, 1988, 1999; Johnson et al., 2016; Muxworthy et al., 2017). Meanwhile, differentiated meteorite parent bodies may have hosted magnetic core dynamos (Weiss et al., 2010). Finally, after the dissipation of the solar nebula ~4 million years (My) after its formation (Wang et al., 2017), magnetic fields of the early solar wind, although potentially much weaker than nebular magnetic fields, may have been recorded in meteorites (O'Brien et al., 2020).

Distinguishing among the possible sources of magnetic field as described above has proven to be difficult even for the most intensively studies chondrites including the Vigarano-type carbonaceous (CV) chondrite Allende. Studies from at least eight laboratories have confirmed that bulk Allende samples, defined as material that contains both matrix and inclusions such as chondrules, carry a strong unidirectional remanent magnetization (Acton et al., 2007; Butler, 1972; Carporzen et al., 2011; Emmerton et al., 2011; Nagata & Funaki, 1983; O'Brien et al., 2020; Sugiura et al., 1979; Wasilewski, 1981). Following Carporzen et al. (2011), we refer to this component of magnetization as the "MT" component for "medium temperature," which refers to the observation that its maximum unblocking temperature is 290 ± 5°C. The strength of the ancient magnetic field that caused the MT magnetization, known as the paleointensity, has been reported to be between 3 and ~100 μT with the majority of values falling between 20 and 60 μT (Table S1). These intensities are potentially consistent with all four classes of magnetic fields outlined above except possibly the solar wind fields, which are likely to be significantly weaker even in case of magnetospheric amplification (Oran et al., 2018).

Understanding the acquisition mechanism of the MT magnetization can provide insight into the ultimate origin of the recorded magnetic field. A thermoremanent or chemical remanent magnetization (TRM or CRM) imparted during metamorphism or aqueous alteration would imply acquisition over 10-10^6 y timescales (Ganino & Libourel, 2020). Such processes could not have recorded impact-generated magnetic fields, which are present for hour to day timescales after an impact (Crawford & Schultz, 1999; Hood & Artemieva, 2008).

The mechanism of remanence acquisition would also influence the interpretation of the paleointensity. Because all three components of solar wind magnetic fields reverse polarity on <<1 year timescales, any solar wind magnetic fields recorded as a CRM or TRM would be attenuated by a factor of ~100 compared to the instantaneous field, further exacerbating the inconsistency between solar wind fields and the observed paleointensity (Oran et al., 2018). For nebular magnetic fields, the reversal of the azimuthal field components on 10^2 or longer year timescales implies that, if the nebular field is recorded over much longer timescales as a metamorphic TRM or CRM, the paleointensity would reflect the projection of the net vertical disk field along the planetesimal rotation axis (Bai, 2017; Fu, Lima, & Weiss, 2014). On the other hand, a shock remanent magnetization (SRM) or impact induced TRM concentrated in the meteorite matrix would be acquired over 1 s timescales (Muxworthy et al., 2017), permitting the recording of impact-generated magnetic fields and nebular magnetic or solar wind fields without attenuation. Determining the mechanism of MT component acquisition is therefore critical for understanding the origin and intensity of the ancient magnetic field.

Close inspection of the MT magnetization's spatial context may provide insight into its mechanism of acquisition. Previous paleomagnetic experiments on separated chondrules and matrix samples have revealed that only the fine-grained matrix and a minority (~20%) of chondrules carry the strong, unidirectional MT magnetization while the remaining chondrules carry only a weaker, non-unidirectional high temperature magnetization that fully unblocks between 330 and 580°C (Fu, Weiss, et al., 2014; Sugiura & Strangway, 1985; Wasilewski & Saralker, 1981).

A viable hypothesis for the origin of magnetization in Allende must explain this unique spatial heterogeneity. A TRM or CRM acquired in a steady nebular or dynamo magnetic field followed by recrystallization of ferromagnetic grains in chondrules may lead to the observed magnetization pattern (Fu, Weiss, et al., 2014). This scenario would predict that ferromagnetic grain populations affected by late-stage alteration would not carry the MT component. Meanwhile, rapid heating of the Allende matrix through impact compression

may have recorded impact-generated magnetic fields while explaining the matrix-chondrule dichotomy in magnetization (Bland et al., 2014; Muxworthy et al., 2017). All grain populations in the matrix would, in this case, carry the MT component. These acquisition mechanisms therefore predict different distributions of the MT magnetization at the grain scale.

Previous studies of Allende were unable to resolve differences in the magnetic records of different grain populations due to limitations in spatial resolution. Here we conduct high-resolution magnetic imaging using the recently developed quantum diamond microscope (QDM) and rock magnetic experiments to identify the ferromagnetic grain populations that carry the MT magnetization and, by extension, assess the mechanism of remanence acquisition. We show that the MT component is carried by Fe-sulfides in the matrix while matrix FeNi metals are non-unidirectionally magnetized. Combined with new rock magnetic experiments characterizing the demagnetization behavior and the thermal and pressure susceptibility of different Allende minerals, we conclude that the MT magnetization was likely a CRM acquired during the alteration of Fe-sulfides in the Allende matrix. Combined with recent geochronology results, we argue that the MT magnetization most likely records a nebular magnetic field within the first 4.2 My of the solar system.

2. Samples and Methods

2.1. Samples

We conducted all experiments on Allende samples extracted from slab AMNH5056 provided by the American Museum of Natural History, at which it had been kept in a cabinet away from magnets but in the Earth's magnetic field since its acquisition by the museum. This parent sample was studied in Carporzen et al. (2011) and Fu, Weiss, et al. (2014) and has been kept in magnetically clean environments (≤200 nT ambient fields) since the previous works. The positive fusion crust baked contact test reported by Carporzen et al. (2011), which demonstrates the preservation of extraterrestrial magnetization in the meteorite interior, therefore applies to our samples. All samples, except those used in pressure remanent magnetization (PRM) acquisition experiments, were mutually oriented to ≤3° accuracy to samples in the previous two studies using saw-cut edges and photomicrographs.

To identify the ferromagnetic mineral populations carrying the MT magnetization, we used reflected light optical microscopy on ~100 μm thick, polished sections of Allende (Figure 1), which allowed us to distinguish FeNi metal, magnetite, pentlandite, and pyrrhotite. Based on our semi-quantitative energy dispersive spectroscopy (EDS) analyses (Figure S2), previous paleomagnetic studies, and our measured Curie temperatures (Fu, Weiss, et al., 2014; Krot et al., 1998), we identify all FeNi metal in our sections as awaruite. We then conducted stepwise thermal demagnetization of natural remanent magnetization (NRM) on the same sections up to 540°C or when the magnetization became erratic.

2.2. Paleomagnetic Experiments

The small, ≤100 μm spatial scale of the individual magnetic sources precludes the use of traditional magnetometers in measuring their magnetic moments. We therefore used a QDM at the Harvard Paleomagnetics Laboratory to perform magnetic field imaging on 11 isolated ferromagnetic sources named A6-A16 after each heating step in projective microscopy mode with a reversing bias field of 900 μT canceled to <0.7 μT and a spatial resolution of 4.7 μm per pixel (Table 1; Fu, Lima, et al., 2020; Glenn et al., 2017). Most sources are between 20 and 100 μm in diameter while one larger extract of matrix material has a diameter of ~700 μm (Figure 1). Each individual source, as demonstrated below, contains ensembles of ferromagnetic grains capable of recording a paleomagnetic field direction. Sample-to-sensor distances were set to between 5 and 60 μm for each source using non-magnetic plastic spacing film.

We then computed the net magnetic moment of each source using a least-squares algorithm in combination with upward continuation in the case of sources A12 and A15 (Table 2). Dipolarity parameters, which measure the fraction of power in a magnetic field map that can be explained by a single fitted dipole, were generally higher than 0.85, implying typical net moment errors of ≤10% in magnitude and ≤8° in angle (Fu,

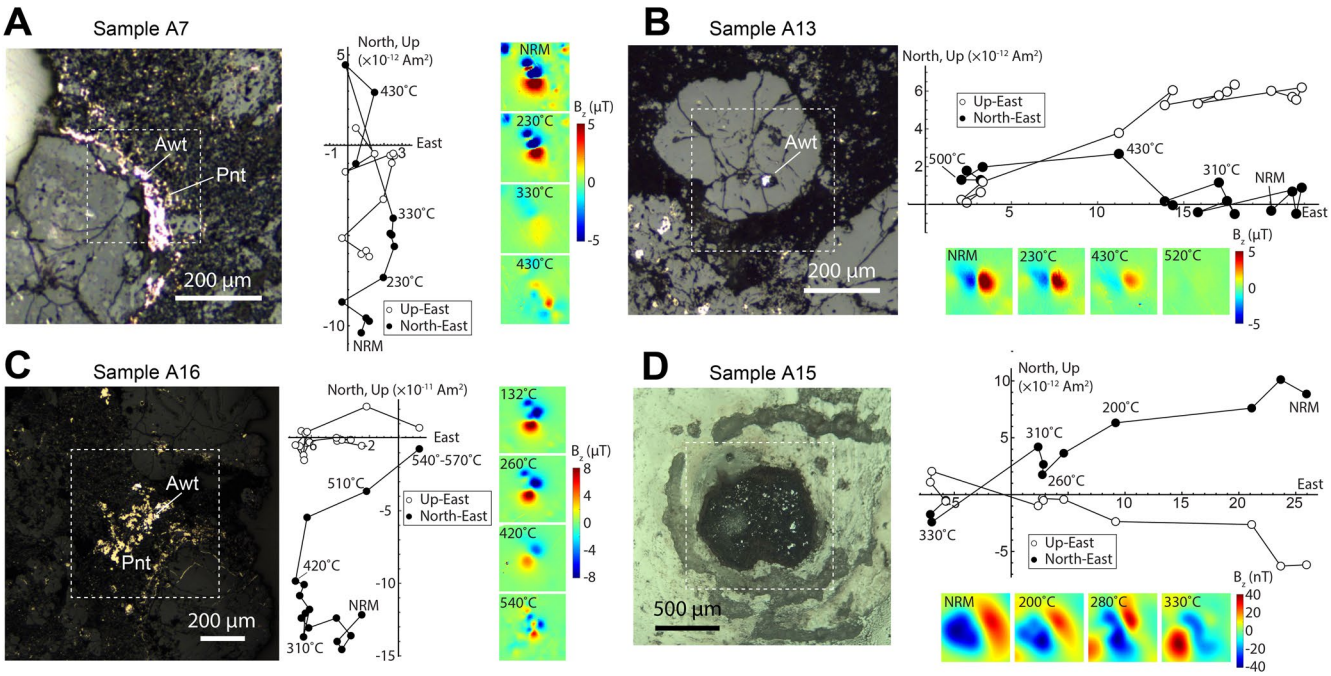

Figure 1. Optical images, demagnetization sequences, and magnetic field maps of four spatially resolved sources in Allende. Left image in each panel is a reflected light photomicrograph with awaruite (Awt) and pentlandite (Pnt) grains highlighted. Dashed square shows the coverage of the corresponding magnetic field map. Middle or upper right image in each panel shows an orthogonal projection (Zijderveld) diagram of the thermal demagnetization sequences. Hollow and solid points denote projection of the magnetization vector onto the vertical and horizontal plane, respectively. Right or lower right image in each panel shows quantum diamond microscope (QDM) magnetic field maps of the source at the indicated demagnetization steps. Magnetic carriers in sample A15 are too fine-grained to image, but are likely sulfides given its demagnetization by ~260°C.

Lima, et al., 2020). Three sources had lower dipolarity parameters of 0.71–0.79, resulting in larger errors of ~15% (Fu, Lima, et al., 2020).

2.3. Rock Magnetic Experiments

To characterize the demagnetization behavior of ferromagnetic grain populations in Allende, we performed thermal demagnetization of an anhysteretic remanent magnetization (ARM) acquired in a 290 mT AC field and 80 μT DC field on 3 sulfide and 2 FeNi-dominated source regions (samples A1–A5). We performed QDM magnetic field mapping and net moment inversions after each heating step as described for NRM samples above.

Table 1
Summary of Experiments and Sample Types Studied in This Work

Experiment	Instrument	Samples	Purpose
Thermal demagnetization of NRM	QDM	11 isolated sources	Identify carriers of MT component
Thermal demagnetization of ARM	QDM	5 isolated sources	Characterize thermal unblocking spectrum of grain populations
Partial TRM acquisition	QDM	1 FeNi-rich source	Test the ability of FeNi assemblages to acquire a partial TRM
Thermal demagnetization of ARM	2G	6 samples (5 matrix; 1 chondrule)	Characterize thermal unblocking spectrum of lithologies
PRM acquisition	2G	1 matrix, 1 chondrule	Determine PRM susceptibility of grain populations
Thermomagnetic cycling	Kappabridge	1 bulk	Identify Curie temperatures and alteration
Low temperature cycling	MPMS	1 bulk	Identify magnetic mineralogy
Semi-quantitative EDS analysis	JEOL 7900F EMP	1 polished section	Identify FeNi composition

Abbreviations: ARM, anhysteretic remanent magnetization; EDS, energy dispersive spectroscopy; EMP, electron microprobe; MPMS, Magnetic Properties Measurement System; NRM, natural remanent magnetization; PRM, pressure remanent magnetization; QDM, quantum diamond microscope; TRM, thermoremanent remanent magnetization.

Table 2
Summary of NRM Samples and Magnetization Components

Number	Context	Mineralogy	Range (°C)	Dec, Inc (°)	MAD (°)	Dipolarity
A6	Chondrule rim	Metal	No comp.			0.79
A7	Chondrule rim	Metal	NRM-430	180.9, 22.2	20.0	0.86
A8	Chondrule rim	Sulfide	NRM-260	149.2, 0.9	15.4	0.87
A9	Chondrule rim	Metal[a]	380–500	204.0, 26.8	11.5	0.92
A10	Chondrule rim	Metal[a]	NRM-500	77.7, −50.9	19.5	0.92
A11	Matrix	Metal	NRM-430	160.8, 71.2	17.9	0.91
A12	Matrix	Metal	NRM-380	9.1, −45.0	14.2	0.94
A13	Chondrule	Metal	NRM-540	95.1, −17.3	14.2	0.89
A14	Chondrule rim	Metal	NRM-540	217.1, 11.0	12.4	0.90
A15	Matrix	Sulfide	NRM-310	74.3, 12.3	7.0	0.71
A16	Matrix	Metal	NRM-290	104.5, 9.1	29.0	0.72
			290–570	211.5, 9.0	16.6	

Note. Context and mineralogy are based on optical microscopy. Range refers to the temperatures over which the magnetization unblocks. Dipolarity parameter is computed from the root-mean-square of the magnetic field map before and after source subtraction and approximates the accuracy of net moment inversions (Fu, Lima, et al., 2020). Samples A1–A5 were subjected to thermal demagnetization after ARM application and are described elsewhere.

Abbreviation: ARM, anhysteretic remanent magnetization; MAD, maximum angular deviation; NRM, natural remanent magnetization.

[a]Superscript 'a' indicates source not present on polished surface but are inferred to be metal due to unblocking temperature range.

We also performed partial TRM and PRM acquisition experiments on different Allende grain populations to test if differences in remanence acquisition efficiency can explain differences in their NRM. We imparted a series of partial TRMs up to 400°C in an 80 μT bias field on an FeNi-dominated region and used the QDM to recover net moments. For PRM acquisition experiments, which are expected to simulate shock remagnetization efficiency within a factor of ~2 (Gattacceca et al., 2010), we pressurized one chondrule, one matrix-dominated, and one larger, oriented bulk sample in a stainless steel cell that has been calibrated in previous studies (Volk & Gilder, 2016). We measured the samples before and after pressure application up to 1.8 GPa in a 200 μT DC field using a 2G Enterprises Model 755 superconducting rock magnetometer (hereafter, 2G).

We further used the 2G to acquire high-resolution demagnetization data to identify mineral Curie temperatures. We performed a thermal demagnetization sequence on 5 matrix-dominated and 1 chondrule samples carrying a 290 mT AC field and 80 μT DC field ARM, which approximates the published paleointensities for the MT component. Based on Carporzen et al. (2011), we used 5–10°C steps between 270 and 325°C and 20–25°C steps between 500 and 590°C to achieve higher resolution near the expected Curie temperatures. We then quantified the Curie temperatures by fitting two sets of hyperbolic tangent and linear functions to the demagnetization curves. We computed the uncertainties on these Curie temperature using a bootstrap resampling approach where we constructed 1,000 synthetic demagnetization sequences based on the variance of magnetizations around the mean for each temperature and fitted each synthetic data set to find the Curie temperature.

To distinguish among different possible Fe-sulfide phases, especially hexagonal and monoclinic pyrrhotite, we obtained thermomagnetic curves of susceptibility as a function of temperature for a bulk Allende sample using an AGICO KLY2 Kappabridge instrument in AC fields of 300 A/m and 920 Hz at the Institute for Rock Magnetism, University of Minnesota. Further, we measured the remanent magnetization of another bulk sample during low temperature cycling of a room temperature (300 K) 2.5 T saturation isothermal remanent magnetization (IRM) to 10 K and back to 300 K on a Quantum Design Magnetic Properties Measurement System (MPMS) both before and after heating to 350°C. Finally, we used a JEOL 7900F electron

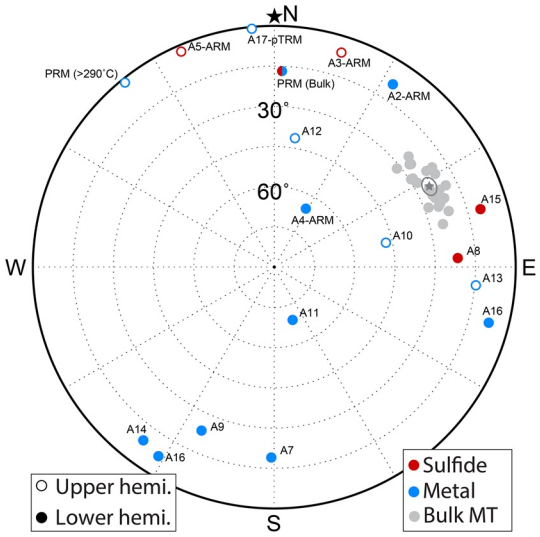

Figure 2. Equal area stereonet projection of fitted magnetization component directions. Red and blue points denote magnetization directions recovered from individual grain assemblages using quantum diamond microscope (QDM) magnetic field maps. All data points are natural remanent magnetization except those labeled "anhysteretic remanent magnetization (ARM)", "partial thermoremanent magnetization", and "pressure remanent magnetization (PRM)". "PRM Bulk" indicates the total PRM acquired by the bulk sample while "PRM > 290°C" indicates PRM remaining after 290°C thermal demagnetization. Black star indicates the bias field direction for both ARM and PRM. Gray points are MT magnetization directions of bulk samples from Carporzen et al. (2011). Gray star and circle indicate the mean and α_{95} confidence interval of the bulk sample directions.

microprobe at the Harvard Center for Nanoscale Systems to conduct compositional analysis on FeNi metal grains using semi-quantitative energy-dispersive spectroscopy.

All data presented here are available from the Harvard Dataverse (Fu, 2020).

3. Results

3.1. Micromagnetic Imaging of NRM

The 11 sources we analyzed using QDM imaging of a stepwise thermal demagnetization represent both awaruite and pyrrhotite carriers in both chondrule and matrix contexts (Table 2). Sources generally show NRM decay commencing below 200°C and extending up to near the Curie temperatures of pyrrhotite and awaruite (Figure 1; see below). We found that 10 sources carry components of magnetization with maximum angular deviation (MAD) ≤20° (Figure 1). Among these, the eight sources associated with awaruite carried component directions that are overall consistent with a random distribution with vector sum length $R_0 = 4.37$ while the critical R for $P = 0.05$ is 5.28 (Figure 2; Watson, 1956). Although one group of four awaruite-hosted component directions belong to a statistically significant cluster with southwesterly declination, we found no independent feature, such as petrographic affinities or location, to justify associating these sources. Further, the clustered direction and its reversed counterpart are not consistent with any identified unidirectional magnetization, including the MT or the poorly defined HT direction reported by (Carporzen et al., 2011). We therefore make no further interpretation of these directions as a cluster and regard the awaruite-hosted component directions as randomly oriented.

Based on the above, we conclude that awaruite sources in all settings, including the matrix, chondrule rim, and chondrule interior, do not carry the MT magnetization despite direct contact with matrix material that hosts the MT component. This conclusion is consistent with the observation of Fu, Weiss, et al. (2014) that ~80% of chondrules, which are rich in FeNi carriers compared to the matrix, do not carry the MT component. Our QDM-based observations extend this conclusion to state that FeNi assemblages within the matrix itself do not carry MT magnetization.

In contrast to the random directions of awaruite-hosted magnetization, the two Fe-sulfide sources measured using the QDM carry magnetization components broadly similar to the bulk MT magnetization direction (Figure 2). The sulfide component farther removed from the bulk MT direction, A8, is separated by 22.3°. The probability of two random directions both coming within 22.3° of a given direction is 0.13%. We therefore reject the hypothesis that the two sulfide directions are random at >99% confidence. The discrepancy between these directions and that of the MT may be due to the low moments of the samples (3.0×10^{-12} and 2.8×10^{-11} Am^2, respectively, for A8 and A15). Our pyrrhotite-dominated samples with similar magnetic moments of ~1.2×10^{-11} Am^2 were able to acquire an ARM in the direction of an 80 μT bias field (Figure 2), implying that sufficient grains are present in the pyrrhotite assemblages to record an ambient field. Even so, samples with similar moments may exhibit statistical errors of order 1° or greater in the case of non-single domain grain distributions (Berndt et al., 2016).

3.2. Rock Magnetic Characterization

Our high temperature resolution thermal demagnetization of ARM-bearing samples revealed two distinct drops in magnetization at 284 ± 6°C and 539 ± 9°C in matrix-dominated samples. Meanwhile, an isolated

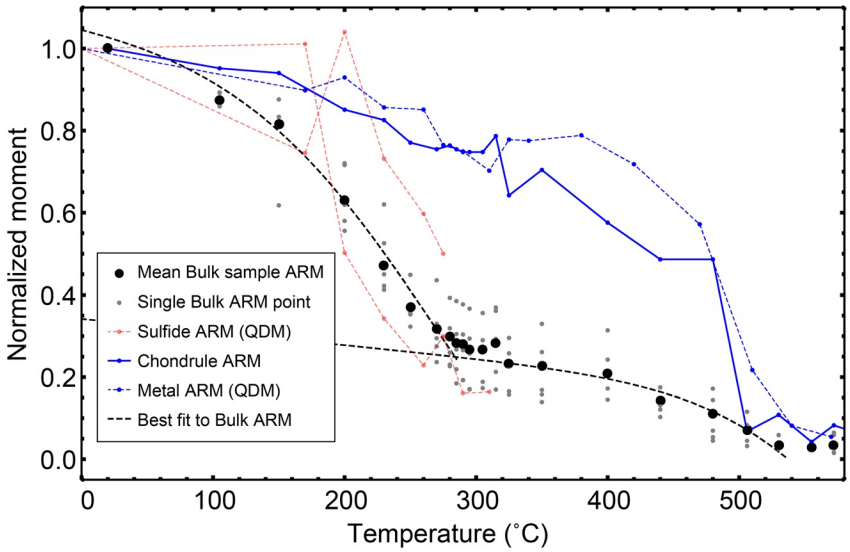

Figure 3. Thermal demagnetization of room temperature laboratory remanence, specifically an anhysteretic remanent magnetization (ARM) acquired in a 290 mT AC and 80 μT DC field. Small gray points are the magnetizations of 5 matrix-rich bulk samples while black points represent their average. Dashed black curves are the best-fit Curie temperature curves for the matrix-rich bulk sample data (see text). Blue solid and dashed curves denote a chondrule and single FeNi assemblage, respectively, which show only a single Curie point. Pink dashed curves are two Fe-sulfide regions mapped using the quantum diamond microscope (QDM). Plotted sequences were truncated at the point where their magnetization lost directional coherence.

chondrule sample exhibited only the higher unblocking temperature (Figure 3). Regarding the 539 ± 9°C transition, in-field thermomagnetic analysis on Allende bulk samples has revealed a Curie temperature at 610°C (Butler, 1972), which is indicative of awaruite and fully consistent with our electron microprobe analysis showing the presence of only high-Ni alloy (Section 3.1; Figure S2). Given, in addition, the observed correspondence between the analyzed magnetic field signals and awaruite (Figures 1 and S1), we conclude that awaruite is the main carrier of high-temperature magnetization unblocking above ~290°C. In this case, the 539 ± 9°C transition observed from demagnetization of ARM may be due to awaruite unblocking significantly below the Curie temperature due to restricted grain size distribution or the destruction of awaruite grains due to alteration at this temperature.

Regarding the observed transition at 284 ± 6°C, previous thermal demagnetization of IRM in Allende has revealed similarly rapid demagnetization at ~290°C; however, the same transition was missing from thermal demagnetization of a 320°C partial TRM (Carporzen et al., 2011; Fu, Weiss, et al., 2014). The presence of hexagonal pyrrhotite, which is a metastable phase with a Curie temperature of 275–295°C and converts to monoclinic pyrrhotite upon heating (Bennett & Graham, 1980), would explain these observations. Although hexagonal pyrrhotite is usually antiferromagnetic at room temperature, observations of pyrrhotite-bearing martian meteorites and terrestrial sediments demonstrate that this pyrrhotite polytype may in fact be ferrimagnetic (see Supporting Information S1; Haines et al., 2019; Horng, 2018; Horng & Roberts, 2018; Rochette et al., 2001).

An alternative interpretation of the 284 ± 6°C transition is that it represents unblocking of monoclinic pyrrhotite below the Curie temperature due to restricted grain size distribution. However, we observe a drop in magnetization at ~290°C in bulk samples as well as fine- and coarse-grained assemblages analyzed with the QDM (Figures 4 and S1). Because this transition does not appear to depend on grain size, it is likely to represent a Curie temperature instead of rapid unblocking below the Curie temperature. Further, the disappearance of this transition and the appearance of a transition at 320°C in samples measured after previous heating to ≥320°C (Figure 4a; Carporzen et al., 2011) is more consistent with a change in mineral Curie temperature after alteration than the transition having a simple grain size-dependent unblocking temperature origin. Although Butler (1972) observes a transition at 320°C during thermomagnetic analysis, conversion

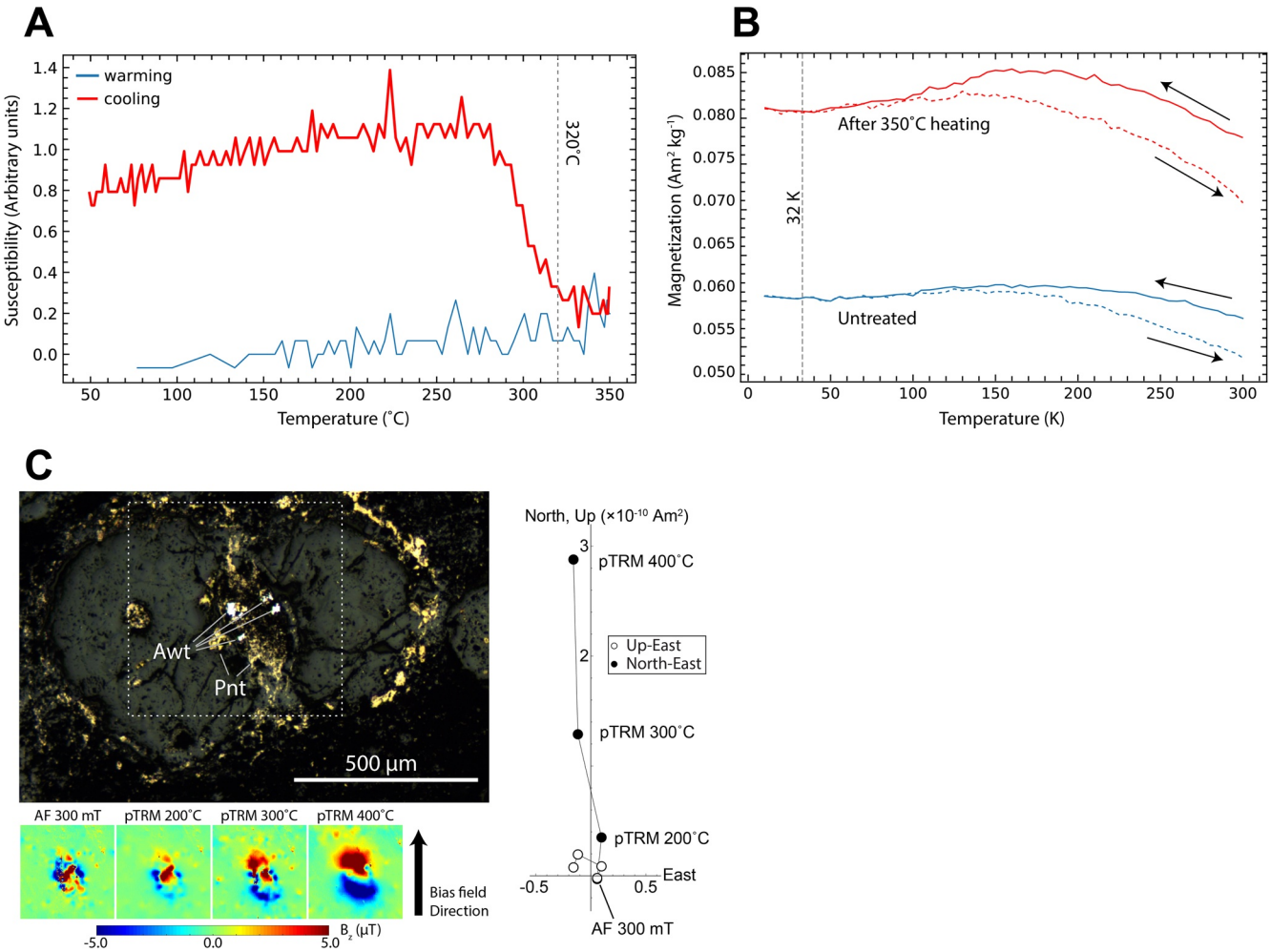

Figure 4. Rock magnetic characterization of Allende grain assemblages. (a) Thermomagnetic analysis showing susceptibility of an Allende bulk sample as a function of temperature during heating and cooling in air. Note the presence of a 320°C Curie temperature after heating to 350°C. The lack of any transitions during warming may be due to the low mass (15 mg) of the sample used, resulting in a low signal-to-noise ratio. (b) Low temperature cycling of an Allende bulk samples before and after heating to 350°C showing the lack of a 32 K Besnus transition in both cases. (c) Partial thermoremanent remanent magnetization (TRM) acquisition on an awaruite assemblage. Quantum diamond microscope (QDM) maps show the magnetic field pattern within the white dashed box. Orthogonal projection diagram shows the fitted net magnetic moment of the source. Laboratory bias field direction is due north in the horizontal plane.

of hexagonal to monoclinic pyrrhotite may occur even on the short timescales of thermomagnetic analyses, as evidenced by our thermomagnetic data that shows a strong 320°C transition upon cooling from 350°C (Figure 4a). Therefore, differences in heating rate can explain the difference between our thermomagnetic experiments and those of Butler (1972). The lack of a Besnus transition at 32 K in both heated and unheated samples (Figure 4b) does not support or rule out the presence of either pyrrhotite polytype as suppression of the Besnus transition has been previously observed in pyrrhotite-bearing meteorites (see Supporting Information S1; Rochette et al., 2001). Combining the above lines of evidence, we conclude that the 284 ± 6°C unblocking temperature observed in Allende matrix material corresponds to the Curie temperature of ferrimagnetic hexagonal pyrrhotite.

A large contrast in the remanence acquisition efficiency of awaruite and pyrrhotite grains can potentially explain our key observation that only the latter population carries the MT component. We therefore conducted ARM, partial TRM, and PRM acquisition experiments on Fe-sulfide and FeNi assemblages. Our QDM imaging of grains subjected to an ARM followed by thermal demagnetization found that two out of 3 sulfides and two out of 2 awaruite assemblages acquired a significant component of magnetization, although the latter showed significant deflection from the bias field direction (Figures 2 and S1). These deflec-

tions are likely due to the inability of the 290 mT ARM AC field to fully remagnetize parts of the FeNi grain population. Although IRM acquisition data shows that only ~10% of remanence-carrying grains in Allende have coercivity ≥300 mT (Fu, Weiss, et al., 2014), isolated FeNi sources can have a much larger fraction of high coercivity grains if the high coercivity magnetization is carried predominantly by FeNi. Remanence anisotropy may also lead to the observed deflection; however, the lack of partial TRM deflection in a FeNi metal source suggests that this carrier population is not strongly anisotropic (see below).

We imparted a partial TRM to one chondrule region containing awaruite and Fe-sulfide at 200, 300, and 400°C in an 80 μT bias field. We identified the Fe-sulfide phase to be nonferromagnetic pentlandite based on reflected light microscopy and the lack of corresponding magnetic field signals (Figures 1a, 1c, and 4c). At the same time, the continued acquisition of partial TRM between 300 and 400°C demonstrates that Fe-sulfide is highly unlikely to be the dominant phase acquiring magnetization. Our thermomagnetic analysis on a bulk sample heated up to 350°C shows that alteration at this temperature is concentrated in the formation of a 320°C Curie temperature phase, which, as discussed above, is related to the decomposition of pyrrhotite instead of oxidation of FeNi metal. The awaruite imaged in Figure 4c therefore did not alter significantly and likely acquired a partial TRM. We therefore conclude that awaruite is capable of acquiring a significant partial TRM parallel to an applied field at temperatures as low as 200°C.

Finally, our PRM acquisition experiments on 1 chondrule and 1 bulk sample showed that the magnetization of the chondrule, which is likely dominated by awaruite (see above and Fu, Weiss, et al., 2014), increased from 3.0×10^{-10} Am^2 to 9.4×10^{-10} Am^2 when cycled to 1.8 GPa hydrostatic pressure in a 200 μT field. The bulk sample was larger and allowed approximately oriented measurements, although the orientation of the sample in the pressure chamber itself is uncertain to ~10°. We found that bulk sample remanence increased by 4.94×10^{-9} Am^2, which is 27% of the sample's NRM intensity, in a direction 19.9° from the bias field direction (Figure 2). After a single thermal demagnetization step to 290°C to isolate the remanence carried by awaruite and Fe-oxide, the remaining remanence differed from the initial demagnetized state by 4.86×10^{-9} Am^2 and was oriented 39.0° from the bias field direction. The discrepancies between the PRMs and bias field direction may be due to a combination of uncertainty in sample orientation in the pressure chamber after the chamber is sealed, the PRM affecting the unremoved high-coercivity remanence initially present in the sample, or inherent PRM anisotropy.

4. Origin of the MT Magnetization in Allende

Our QDM-based magnetic imaging has revealed that awaruite assemblages in both the matrix and chondrules of Allende do not carry the MT magnetization component. At the same time, the same awaruite assemblages are capable of acquiring magnetization under heating and pressure application. Thermal demagnetization of NRM and ARM demonstrates that significant awaruite-hosted remanence is unblocked in the 200–300°C range over which the MT component is blocked (Figures 1 and 3), indicating that a grain size distribution without remanence unblocking ≤290°C cannot account for the lack of the MT magnetization carried by awaruite. Further, the existence of well-defined, awaruite-hosted magnetization components blocked over several hundred degrees up to 540°C is inconsistent with viscous removal of magnetization in awaruite since viscous evolution in the presence of very weak post-nebular asteroid belt magnetic fields would remove identifiable component directions. We therefore conclude that the lack of MT magnetization in Allende metal requires a nonthermal origin of the MT component or later, preferential removal of the MT magnetization from FeNi carriers. We explore these possibilities in detail below, organizing our discussion around the process that led to the initial acquisition of the MT component.

4.1. MT Magnetization as a Partial TRM

Proposed partial TRM models for the MT magnetizations invoke both radiogenic (Carporzen et al., 2011) and impact heat sources (Muxworthy et al., 2017). Both scenarios predict that all ferromagnetic grain populations in the matrix should initially carry the MT component. However, our observation that awaruite in both the matrix and chondrules lack the MT component requires complete subsequent removal of this magnetization from FeNi minerals, possibly due to their later formation during aqueous alteration (Fu,

Weiss, et al., 2014). As discussed below in Section 4.2, complete chemical removal of MT magnetization from FeNi grains is unlikely.

A strong argument previously advanced in favor of the partial TRM hypothesis is that the 290 ± 5°C maximum unblocking temperature of the MT component is resolvably lower than the 320°C Curie temperature of monoclinic pyrrhotite. However, our experiments show the existence of a Curie point at 284 ± 6°C, which we interpret as evidence for ferrimagnetic hexagonal pyrrhotite (Figure 3). Because heating to higher temperature or chemical remagnetization can result in remanence blocked up to the Curie point, this finding obviates the main evidence in support of a partial TRM origin.

In addition, an impact-induced partial TRM must explain the observation that the maximum unblocking temperature of the MT component appears uniform within ~20°C throughout the Allende matrix (Carporzen et al., 2011; Fu, Weiss, et al., 2014; Nagata & Funaki, 1983; Sugiura et al., 1979). This uniformity contrasts with the ≥100°C spread in matrix maximum heating temperatures due to impact compression (Bland et al., 2014; Muxworthy et al., 2017). For these reasons, we conclude that the MT magnetization is unlikely to be a 290°C partial TRM.

4.2. MT Magnetization as a Full TRM

In the case of radiogenic or impact heating above 284 ± 6°C, pyrrhotite would have acquired a full TRM while other phases with higher Curie temperatures would have acquired a partial to full TRM immediately after the heating event.

This interpretation has two potential challenges. First, as in the case of a partial TRM origin, a later event is required to remove the MT component from awaruite. Fu, Weiss, et al. (2014) invoked heterogenous aqueous alteration affecting awaruite to explain the lack of MT magnetization in most chondrules. A key assumption of this model is that a significant time delay existed between the formation of the Fe-sulfides and awaruite. Both mineral populations in Allende formed during aqueous alteration, specifically due to sulfidation and oxidation of primary, low Ni content FeNi metals. The timing of these reactions may have been near the beginning (Krot et al., 1998, 2004) or the end (Ganino & Libourel, 2017) of the aqueous alteration sequence. In either case, the formation of Fe-sulfide and awaruite is expected to have been contemporaneous or associated with a short delay of $<10^2$ years (Ganino & Libourel, 2020).

Fu, Weiss, et al. (2014) conjectured that the higher permeability of the porous matrix compared to chondrules led to faster and therefore earlier aqueous alteration, leading to a time difference between the formation of the final ferromagnetic assemblages in the matrix and chondrules. However, our results show that awaruite in the matrix also do not carry the MT magnetization, contradicting the permeability-dependent alteration hypothesis. Observations that Fe-sulfide and FeNi metal assemblages in chondrule and matrix contexts are compositionally indistinguishable further supports their contemporaneous formation (Blum et al., 1989). Further, some awaruite that lack the MT magnetization are observed intergrown with Fe-sulfides (Figures 1a and 1c), suggesting that the two grain populations are co-genetic. We therefore find no compelling independent evidence to support a time delay between the formation of MT-carrying pyrrhotite and MT-lacking awaruite populations.

A second challenge to a TRM origin for the MT magnetization is that, if the host mineral phase is hexagonal pyrrhotite as suggested by its 290°C maximum unblocking temperature (see above), cooling from >290°C is expected to have destabilized these metastable carriers as observed in our thermomagnetic experiments (Figure 4). Laboratory experiments show that at least some inversion of hexagonal pyrrhotite to the monoclinic form is expected to occur during cooling through ~250°C for Fe-S compositions in the range observed for Allende Fe-sulfides (46.63–48.90 atomic % Fe; Blum et al., 1989; Haggerty & McMahon, 1979; Kissin & Scott, 1982).

In summary, a TRM origin for the MT magnetization would require a specific sequence of events with heating occurring after Fe-sulfide formation but before awaruite formation. This alteration and heating sequence is not supported by petrologic observations. At the same time, the hexagonal pyrrhotite carrier of the MT should not have survived heating to the >300°C temperature required for imparting a TRM. We therefore conclude that the MT magnetization is highly unlikely to be a TRM.

4.3. MT Magnetization as a Shock Remanent Magnetization (SRM)

Impact shock in the presence of a magnetic field can impart an SRM (Gattacceca et al., 2008). A non-thermal origin for the MT magnetization may explain its absence in awaruite carriers because the susceptibility of different minerals to non-thermal magnetization processes may vary widely. Due to the possible existence of multiple pressure-induced phase transitions in pyrrhotite below the 5 GPa maximum shock pressure of Allende (Alexander et al., 2007; Rochette et al., 2003), Fe-sulfide in Allende may have been especially susceptible to acquiring remanence compared to FeNi metals.

However, the complete lack of MT magnetization in FeNi metals requires that these grains have virtually no susceptibility to SRM acquisition. Our PRM acquisition experiments, which provides an estimate for SRM susceptibility, showed that chondrules and non-Fe-sulfide grains are able to acquire substantial magnetization during pressure cycling, although with potentially significant anisotropy. However, even large anisotropies cannot replicate the randomly distributed NRM component directions observed in awaruites. We therefore conclude that the absence of the MT magnetization in FeNi grains cannot be explained by impact shock.

4.4. MT Magnetization as Magnetization Related to Atmospheric Entry

We further consider the possibility that warming or pressurization of Allende material during Earth atmospheric entry resulted in a record of the Earth's magnetic field (Kletetschka, 2018). Although this previous study reported a change in the magnetization of three chondrules during heating in an Earth-strength field between 150 and 270 K, only two of the three samples in fact gained in magnetic moment. In these cases, the change in magnetic moment in this temperature range was <7% of the NRM intensity. True temperature change in the presence of the Earth field during atmospheric entry was likely significantly less than the 120 K used in the experiment because the blackbody temperature of the Allende meteoroid at 1 AU is ~253 K (de Pater & Lissauer, 2010). Therefore, although an inverse TRM during atmospheric entry may have modified Allende's magnetization, it is more than an order of magnitude too weak to explain the MT component. Further, the mineralogy of Allende chondrules on which the previous inverse TRM experiments were based differ markedly from that of the matrix, which is the predominant carrier of the MT component (Figure 3; Fu, Weiss, et al., 2014). The Kletetschka (2018) study further suggested that uniaxial stresses of ~18 MPa was sufficient to cause remanence acquisition during arrival on Earth. However, no published dynamic or static high pressure magnetization experiments have shown that such low pressures can result in a change in magnetization consistent with the MT component (e.g., Ohnaka & Kinoshita, 1968; Volk & Gilder, 2016). We therefore conclude that the MT component is not the result of modification during atmospheric entry.

4.5. MT Magnetization as a Chemical Remanent Magnetization (CRM)

Textural and isotopic evidence provides strong support for the formation of Fe-sulfide, Fe-oxide, and FeNi metal phases in Allende during aqueous alteration on the parent body (Brearley, 2006; MacPherson & Krot, 2014). Therefore, all ferromagnetic phases in Allende may have acquired a CRM provided the existence of a significant magnetic field and a sufficiently high efficiency of CRM acquisition. Experimental studies have shown that the efficiency of CRM acquisition is highly dependent on the mineralogy, reaction pathway, and intergrowth relationships involved and may be positive, zero, or negative (Garming et al., 2007; Heider & Dunlop, 1987; McClelland & Goss, 1993; Stokking & Tauxe, 1990). Although no experiment of CRM acquisition has been performed on the sulfidation of FeNi metal, the frequent observation of CRM in diagenetic pyrrhotite on Earth supports the possibility that Allende Fe-sulfides could acquire a strong CRM (Roberts & Turner, 1993; Weaver et al., 2002).

Meanwhile, the absence of the MT magnetization in awaruite assemblages can be explained if pyrrhotite has a much higher efficiency of CRM acquisition than awaruite. Therefore, unlike the TRM scenario described above, a CRM origin would not require a time delay between the formation of the two grain populations, which is consistent with the expected alteration sequence (Ganino & Libourel, 2020; Krot et al., 1998, 2006). Furthermore, a CRM may be acquired in a low temperature environment; therefore, metastable hexagonal

pyrrhotite carrying the MT component would have avoided transformation to the monoclinic form during heating if the aqueous alteration post-dated any ≥300°C heating events.

A key assumption required by the CRM origin hypothesis is that the CRM acquisition efficiency of pyrrhotite is much higher than that of awaruite. Although no direct CRM acquisition experiments exist for any of the chemical transformations in Fe-bearing Allende phases, the presence of a CRM in only a subset of minerals within a set of rock samples is well-documented with some instances showing pyrrhotite retaining a distinct magnetization compared to Fe-oxide phases (Xu et al., 1998; Zegers et al., 2003). Further, theoretical consideration TRM acquisition efficiency, defined as the ratio of a TRM acquired in a given field to the saturation remanent magnetization, shows that the efficiency of TRM acquisition in pyrrhotite is ~1 order of magnitude higher than in FeNi metal due to the lower saturation magnetization of the former (Kletetschka & Wieczorek, 2017; Kletetschka et al., 2004). For a grain growth CRM scenario, the dependence of the efficiency on the saturation magnetization is expected to be similar (compare (Equation 1) in Kletetschka et al., 2004 and (Equation 1) in McClelland, 1996). Due to the similarly low saturation magnetization of hexagonal pyrrhotite (Horng, 2018), these conclusions likely apply equally to Allende pyrrhotite. We therefore find that large differences in CRM acquisition efficiency among ferromagnetic minerals populations in Allende are plausible, although future experiments of CRM acquisition using the appropriate starting compositions and oxygen and sulfur fugacity environments would be required to fully test this scenario.

Finally, a CRM resulting in pyrrhotite grains with unblocking temperatures between ~200 and 290°C should be stable to viscous decay over solar system timescales. Grains that unblock at ~200°C in the laboratory would have been viscously relaxed in 4.5 billion years only at temperatures of 120°C, which is far warmer than equilibrium blackbody temperature between the Earth and the asteroid belt (Carporzen et al., 2011).

4.6. Timing of the MT Magnetization

Based on the above discussion, we conclude that the MT magnetization is most likely a pyrrhotite-carried CRM. In this case, the acquisition of the MT component would have coincided with the formation of pyrrhotite during parent body alteration. Because pyrrhotite from CV chondrites has not been directly dated, determining its age requires understanding the relative timing of its formation relative to datable secondary phases.

Two sequences for aqueous alteration in Allende have been proposed. First, pre-accretional, low-Ni metal may have transformed to Fe-oxides, Fe-sulfides, and high-Ni metal, which in turn altered to form Fe-bearing silicates such as fayalite and andradite (Krot et al., 1998, 2004). In this case, the timing of Fe-sulfide formation would have pre-dated both peak metamorphism and the formation of Fe-bearing silicates. Alternatively, Fe-bearing silicates may have formed first during high temperature (≥400°C) alteration, after which Fe-oxides, Fe-sulfides, and awaruite formed during late stage cooling in analogy with fumarolic hydrothermal alteration on Earth (Blum et al., 1989; Ganino & Libourel, 2017, 2020). Pyrrhotite in this scenario would have formed at between 300 and 150°C after peak metamorphism (Alt et al., 2007; Klein & Bach, 2009).

An important requirement for a CRM origin for the MT component is that no metamorphism above the 284°C apparent Curie temperature is permitted after pyrrhotite formation. Therefore, our interpretation of the MT component as a pyrrhotite CRM requires the sequence of events described in Ganino and Libourel (2017, 2020) where pyrrhotite formation post-dates peak metamorphism.

In addition to allowing the preservation of a pyrrhotite CRM, this alteration model also holds key implications for the timing of pyrrhotite formation. Unlike in a one-dimensional onion shell model of chondrite metamorphism, zones of alteration in the fumarolic model are highly localized, possibly associated with igneous intrusions or permeability conduits for hot metasomatic fluids. This setting is analogous to hydrothermal systems on Earth, which start with a source of sub-surface heat, establish seawater circulation, and wane over time as the heat source is exhausted and the permeability of the system is modified (Lowell & Germanovich, 1994).

Consequently, the time delay between the formation of datable secondary Fe-bearing silicates (e.g., fayalite) and pyrrhotite in the fumarolic alteration framework is expected to be short, possibly on the order of

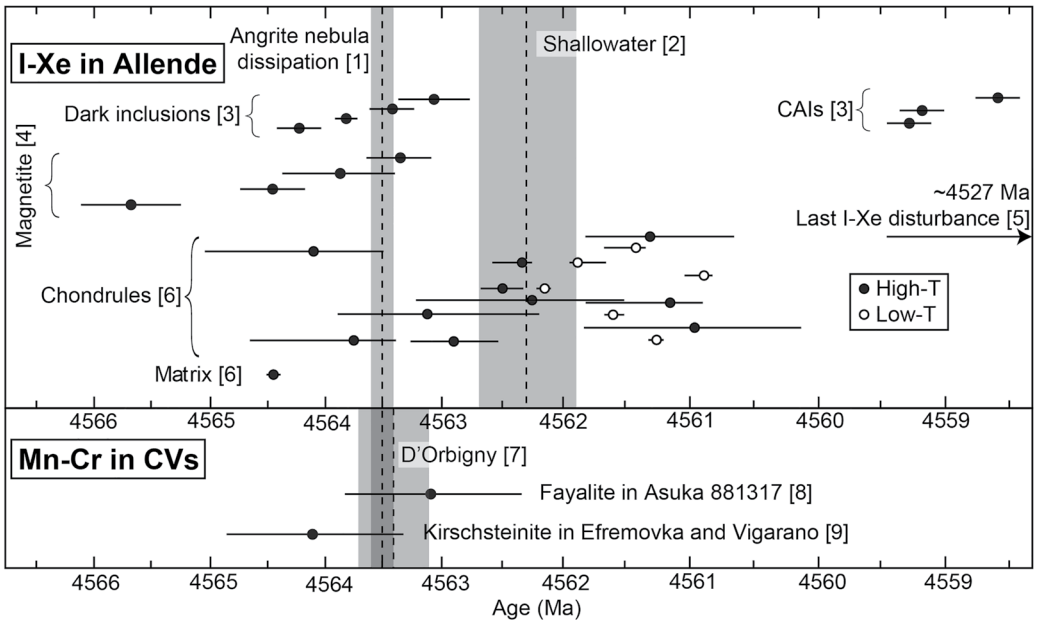

Figure 5. Summary of radiometric dating of aqueous alteration in Vigarano-type carbonaceous (CV) chondrites. Absolute age and 2σ range of the Shallowater aubrite and D'Orbigny angrite, which are used to anchor the I-Xe and Mn-Cr systems, are shown to indicate magnitude of additional uncertainty introduced when comparing ages produced by the two systems. References: (a) Wang et al. (2017); (b) Gilmour et al. (2009); (c) Pravdivtseva et al. (2003); (d) Pravdivtseva et al. (2013); (e) Carporzen et al. (2011); (f) Swindle et al. (1983); (g) Glavin et al. (2004); (h) Doyle et al. (2015); (i) MacPherson et al. (2017).

10 years by analogy with terrestrial fumaroles (Ganino & Libourel, 2020). Other chondrite studies have provided evidence for parent body alteration in such rapid, fumarole-like systems. In the case of the L6 chondrite Villalbeto de la Peña, large surviving isotopic gradients indicate that the meteorite was brought up to ~800°C and cooled, possibly multiple times, each in the span of 1–10 years (Dyl et al., 2012). For Allende itself, a study of diffusion profiles in olivine and pyroxene in the matrix found micrometer-scale Fe-Mg compositional gradients that correspond to heating times of 10^2 to 10^5 y (Cuvillier et al., 2015).

These short timescales for the alteration cycle imply that the age of secondary Fe-bearing silicates can be directly interpreted as the age of pyrrhotite and of the MT component. Although no such mineral from Allende has been analyzed to-date, fayalite and kirschsteinite in reduced and Bali-type oxidized CV chondrites have been dated to $3.2^{+0.8}_{-0.7}$ and $4.2^{+0.8}_{-0.7}$ My after calcium aluminum-rich inclusions (CAIs), respectively (Figure 5; Doyle et al., 2015; MacPherson et al., 2017).

A more direct constraint on the formation age of Allende Fe-sulfides potentially comes from the ^{129}I-^{129}Xe decay system. Early studies of Xe isotopic composition in Allende components showed that the matrix, which hosts the MT remanence, and dark inclusions underwent alteration within 3.0–4.1 My of CAIs (Figure 5; Pravdivtseva et al., 2003; Swindle et al., 1983). Later thermochronological reanalysis of Allende I-Xe data suggested that some alteration of Allende material continued until ~40 My after CAIs (Carporzen et al., 2011). However, the main carrier phase or phases of iodine in Allende matrix and chondrule material have not been conclusively identified. The relationship between I-Xe ages of bulk Allende material and the formation of ferromagnetic assemblages therefore remains uncertain.

I-Xe ages have also been recovered from four magnetite extracts taken from bulk Allende material and published in a conference proceedings (Pravdivtseva et al., 2013). Because magnetite and pyrrhotite occupy the same stage in the alteration sequence regardless of the alteration model (Ganino & Libourel, 2017; Krot et al., 1998), these magnetite ages likely represent the most direct constraints on the timing of pyrrhotite formation. The four magnetite extracts have I-Xe ages between 1.6 and 4.0 My after CAI formation with a mean of 3.0 ± 0.5 My (Figure 5).

Based on the above, we conclude that 3.0 ± 0.5 My after CAIs is the most probable age for pyrrhotite in Allende, while secondary silicate ages of 3.2–4.2 My after CAIs provide a lower bound. Our estimated age for Allende magnetization is significantly earlier than the ~5–40 My after CAIs figure adopted by earlier studies for three principal reasons (Carporzen et al., 2011; Fu, Weiss, et al., 2014). First, our interpretation of a CRM as the most likely form of magnetization means that the magnetization must have the same age as the growth of the carrier phase. In contrast, a partial TRM as hypothesized in previous studies can be imparted during any heating event post-dating carrier mineral formation. Second, due to the recognition of biases in Cr isotopic sensitivity caused by mineral Fe content, Mn-Cr ages of secondary Fe silicates in Allende have been revised upward from 5 to 8 My to 3.2–4.2 My after CAIs, thereby placing a stricter lower bound on the age of Fe-sulfides (Doyle et al., 2015; Hutcheon et al., 1998). Third, I-Xe ages of Allende magnetite, which show formation at 3 My after CAIs, were not available at the time of earlier paleomagnetic studies (Pravdivtseva et al., 2013).

4.7. Origin of the Magnetizing Field

The age of the MT magnetization, which is constrained as a result of this work due to its identification as a CRM, has strong implications for the origin of the recorded field. Studies of CM chondrites suggest that magnetic fields in the solar nebula persisted to >3 My after CAIs (Bryson et al., 2019; Cournede et al., 2015). Further, the presence of fine-grain dust in CR chondrites that formed ≥3.7 My after CAIs supports the presence of nebular gas until at least that time (Fu, Kehayias, et al., 2020; Schrader et al., 2017). Low magnetic field intensities recorded in angrites suggest at least local depletion of nebular gas by 3.8 My after CAIs (Wang et al., 2017). Therefore, the MT magnetization dated to 3.0–4.2 My after CAIs was therefore likely acquired in the presence of nebular magnetic fields.

Alternative origins for the magnetic field recorded in Allende include an internally generated dynamo. A recent thermal evolution model found that a core dynamo on planetesimals is likely to be delayed until ~5 My after CAIs, although dynamo initiation at 4.2 My is possible for small, early accreting bodies (Bryson et al., 2019). However, these models assume an instantaneously separated core and a one or two-stage accretion history.

An updated study by Dodds et al. (2021) includes a time-resolved model of core segregation accounting for thermally driven changes in the density of newly descended Fe-S melt. The models also consider a wide range of accretion timescales between instantaneous to several million years. With these refinements, the Dodds et al. (2021) conclusions remain similar to those of Bryson et al. (2019), suggesting that only a highly specific scenario with a very small body and a narrow range of intermediate accretion rates can achieve a core dynamo by 4 My after CAIs. In any case, bodies with a substantial unmolten chondritic lid that could have sourced the CV chondrites do not form dynamos. The inclusion of core stratification makes an early dynamo more difficult compared to the Bryson et al. (2019) models as early-formed, fast accreting planetesimals develop with stable thermally stratified cores. Finally, both theoretical studies assume that ^{26}Al stays well-mixed in the magma ocean and is not efficiently erupted to the surface as argued by Neumann et al. (2014). As such, these models represent an optimistic case for generating an early planetesimal dynamo.

One additional uncertainty regarding the timing of a chondrite parent body dynamo is the possibility of convection driven by the descent of denser, Fe-rich melts evolving under equilibrium melting. Due to the rapid decay of ^{26}Al, the magma ocean within modeled planetesimals reaches a maximum temperature in less than 10^5 y after first silicate melting (Dodds et al., 2021). Any Fe-S melt segregating during this time may evolve toward a more Fe-rich composition, introducing denser melts into the core that can potentially drive convection. However, this interval is brief and precedes the accretion of the Allende meteorite by more than 1 My. Subsequent Fe-S melt may be produced by progressive upward melting of the overlying chondritic material, especially in the case of continual accretion. However, newly formed Fe-S melt sinking through the magma ocean would no longer evolve as an equilibrium melt once it has been separated from its source region. This melt would enter the magma ocean with a composition corresponding to the lower temperature regions from which the melt was extracted, which would result in less Fe-rich melts than the

core. As such, this mechanism is unlikely to change the conclusions of the Bryson et al. (2019) and Dodds et al. (2021) works, especially for the most relevant interval 3.0–4.2 My after CAIs.

In parallel, several paleomagnetic studies have found possible experimental evidence for a delayed core dynamo in planetesimals. Magnetite in the Kaba CV chondrite is unmagnetized between its Curie temperature (580°C) and 250°C, below which a magnetization component ~3 μT paleointensity can be observed (Gattacceca et al., 2016). Although the nominal paleointensity of 3 μT is highly uncertain, the existence of any identifiable component of magnetization at <250°C contrasts clearly with the lack of unidirectional magnetization at highly temperatures. The authors concluded, based on the lack of a CRM blocked up to the Curie temperature, that there was no appreciable magnetic field on the CV parent body at ~4 My after CAIs when the magnetite formed during aqueous alteration. Meanwhile, the <250°C component recorded a late-starting parent body dynamo at a younger age. In this scenario, the contrast between a nebular field-induced CRM in Allende and the lack of such a CRM in Kaba may result from a difference in the timing of alteration, possibly combined with fluctuations in the nebular field intensity (Riols & Lesur, 2019).

At the same time, the paleomagnetic record of angrites may also provide evidence for a delayed dynamo. Wang et al. (2017) argues that volcanic angrites crystallized in a <0.6 μT magnetic field at 4–6 My after CAIs; meanwhile the later-formed Angra dos Reis meteorite recorded a ~17 μT magnetic field at 11 My after CAIs (Weiss et al., 2008). Summarizing these theoretical and experimental lines of evidence, an active dynamo on the CV parent body is unlikely to have existed at the time of Fe-sulfide formation at 3.0–4.2 My after CAIs. In contrast, this age range of formation overlaps strongly with the lifetime of the solar nebula (Figure 5), leaving a nebular field as the most likely candidate for the magnetization field of the MT component.

The 3.0–4.2 My after CAI age of magnetization would have likely been too early to record solar wind magnetic fields, as solar wind magnetic fields are expected to have only extended out to ≤0.1 AU in the presence of partially magnetized nebular gas (Shu et al., 1997). Finally, because alteration in Allende occurred over extended timescales of 10–10^6 yr (Ganino & Libourel, 2020; Krot et al., 2006), the MT magnetization could not have recorded impact generated magnetic fields that persist over hours to days timescales (Crawford & Schultz, 1999).

5. Implications for Nebular Magnetism

Based on the reasoning above, we conclude that a CRM recording a nebular magnetic field at 3.0–4.2 My after CAIs is the most likely origin of the MT magnetization in Allende although a dynamo field cannot be ruled out. The impact of this result on our understanding of disk processes depends on the paleointensity of the MT component and on the location of the CV parent body when the field was recorded.

Previous studies of Allende have produced paleointensity estimates between 25 and 100 μT for the MT component based on Thellier-Thellier dual heating and room temperature normalization methods (Table S1; Carporzen et al., 2011; Emmerton et al., 2011; Sugiura et al., 1979). All of these protocols assume a TRM origin for the magnetization. Recovery of paleointensity from a CRM such as the MT component is highly uncertain because the CRM acquisition efficiency depends strongly on reaction pathway, grain size, and grain-scale magnetostatic interactions that are difficult to characterize for a particular sample (e.g. Heider & Dunlop, 1987; Özdemir & Dunlop, 1985; Stokking & Tauxe, 1990). Furthermore, CRM acquisition in Fe-sulfides remains less studied compared to in Fe-oxides. In particular, the room temperature remanence carrying capacity of hexagonal pyrrhotite was not appreciated until recently (Horng, 2018; Horng & Roberts, 2018; Rochette et al., 2001); as such, no experimental constraints on its CRM acquisition efficiency exists. Future studies of NRM carried by hexagonal pyrrhotite, such as in methane seep sediments, would permit first-order calibration of its paleointensities.

Here we use CRM efficiencies obtained for other ferromagnetic minerals to compute an order-of-magnitude estimate for the paleointensity of the MT magnetization. The ratio of CRM to TRM acquisition efficiency (χ_{CRM}/χ_{TRM}) varies from 0 (i.e., ambient field has no impact on resulting remanence) to ~1 for a broad set of ferromagnetic minerals including titanomagnetite, maghemite, and hematite (Heider & Dunlop, 1987; Özdemir & Dunlop, 1985; Stokking & Tauxe, 1990). If the efficiency of CRM acquisition in hexagonal pyrrhotite falls within this range, that would suggest that the mean of published paleointensities for the

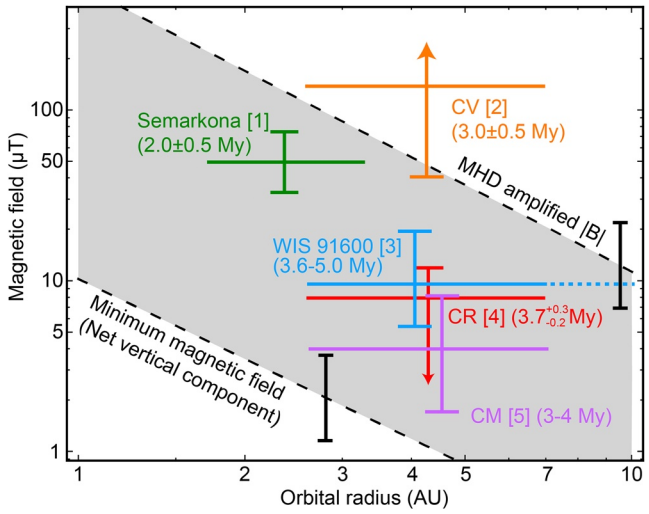

Figure 6. Magnetic field intensities of the solar nebula inferred from chondritic meteorites (CM) and magnetohydrodynamical (MHD) simulations. Minimum theoretical magnetic field (lower dashed line) is the net vertical field required to sustain mass transport at 10^{-18} M_{Sun} yr^{-1} (Bai, 2015). Black error bars on the dashed lines result from a 1 order of magnitude uncertainty on the solar accretion rate. The upper dashed line corresponds to an amplification factor of 60 due to a disk dynamo (Bai, 2017). Field uncertainties on meteorite data are 1σ and include contribution from unknown parent body rotation axis for Vigarano-type carbonaceous (CV), WIS 91600, and CM. Lower bound on Allende paleointensity is based on amplifying the 20 μT of Carporzen et al. (2011) by 2 due to spin axis-magnetic field misalignment. The upper bound is poorly constrained due to the possibilities of low chemical remanent magnetization (CRM) acquisition efficiency, nebular field variability, and pressure demagnetization (see text). Orbital distance uncertainties are from consideration of the snow line and deuterium to hydrogen ratios (see Section 5). Meteorite references: (a) Fu, Lima, and Weiss (2014); (b) This work; (c) Bryson et al. (2020); (d) Fu, Kehayias, et al. (2020); (e) Cournede et al. (2015).

MT component, which is 61 ± 15 μT (Table S1), represents a minimum value for the true ancient field. The occurrence of impacts depressing the preserved paleointensity would further support interpretation of this paleointensity as a lower bound (Volk & Gilder, 2016).

A further implication of a CRM origin of the MT component is that the timescale of acquisition (>10s of years; see above) is much longer than the rotational period of the body. As such, the recorded paleointensity represents the projection of the true nebular field on the spin axis of the CV chondrite parent body. We therefore assume that the spin axis is randomly oriented with respect to the magnetic field and, because the ratio between the true and recorded field intensity is not normally distributed, use Monte Carlo resampling to generate the expected distribution of nebular field strength. Because this quantity is also not normally distributed, we report the result as the median. From this effect, the best-guess and lower bound MT component paleointensity of 61 μT and >20 μT, respectively, become amplified to 122 and > 40 μT (Figure 6). Depending on the timescale of CRM acquisition compared to that of magnetic field reversals in the disk, this value may be the total magnetic field or its net vertical component. Rapid alteration in a fumarole-like environment would predict CRM acquisition in as little as ~10 years, shorter than the expected field reversal timescale of 10^2–10^3 yr (Bai, 2015; Ganino & Libourel, 2020), implying that the 122 μT best-guess and >40 μT minimum values are a constraint on the total magnetic field.

This paleointensity likely represents the nebular magnetic field strength within 0.1 scale height of the midplane at an orbital radius between 2.5 and 7 AU based on the presence of water and hydrogen isotopic data (Fu, Kehayias, et al., 2020; Min et al., 2011; Sutton et al., 2017). Adopting these constraints on the physical location, the minimum paleointensity of 40 μT can be compared to expected field strengths from magnetohydrodynamical (MHD) simulations and to the paleomagnetic record from other carbonaceous chondrites (Figure 6). The MT component paleointensity is much greater than the 1–4 μT net vertical magnetic field required for mass and angular moment transport, assuming a magnetocentrifugal wind mechanism (Bai, 2015). This high paleointensity may be due to amplification of the net vertical magnetic field through the Hall shear instability, which may increase the total field strength by a factor of 10–60 (Bai, 2017; Weiss et al., 2021).

Alternatively and not mutually exclusively, a wind-driven accretion rate about an order of magnitude larger than the canonical 10^{-18} M_{sun} y^{-1} may also explain the high paleointensity. Such a high outer solar system accretion rate would be consistent with the high ejection efficiency expected for disk winds, which results from the progressive depletion of inward flowing material through these winds (Lesur, 2021). The existence of such strong, Hall effect amplified fields may affect the efficiency of gas-mediated planet migration in the early solar system, although its quantitative effects have not been fully explored (Baruteau et al., 2014).

The ≥40 μT Allende paleointensity is significantly stronger than the ≤10 μT values recovered from other outer solar system meteorites such as CM and CR group chondrites and the ungrouped chondrite WIS 91600 (Bryson et al., 2019, 2020; Cournede et al., 2015; Fu, Kehayias, et al., 2020). Although the age of the Allende magnetization may pre-date these other records, the temporal difference is likely less than 1 My. Secular depletion of the solar nebula during this interval probably cannot fully account for the large paleointensity contrast.

Instead, we propose that the large discrepancy between paleointensities recovered from Allende and from other carbonaceous chondrites provides evidence for temporal variation or spatial heterogeneity in the outer solar nebula due to planet formation or MHD instabilities. MHD simulations suggest that magnetic fields

and gas density may fluctuate by more than one order of magnitude on the 10^2 orbit timescale (Bai, 2015), which is sufficient to account for the full range of carbonaceous chondrite-derived paleointensities.

At the same time, observations of pervasive ring and gap structures in other PPDs from the Atacama Large Millimeter Array (ALMA) have motivated theoretical investigation into their origin (ALMA Partnership et al., 2015; Andrews et al., 2018). Hypothesized mechanisms for the formation of rings and gaps include gravitational interactions with giant planets and MHD-induced self-organization of magnetic fields (Dipierro et al., 2016; Krapp et al., 2018; Riols & Lesur, 2019; Riols et al., 2020; Suriano et al., 2018). In the latter case, magnetic field strengths are expected to vary by factor of several over <1 AU length scales. In the case of gaps caused by giant planet formation, MHD simulations also predict nearly order of magnitude variations in magnetic field intensity within several 0.1 AU distances of the accretion planet (Gressel et al., 2013). Therefore, the opening of gaps by either planet formation or MHD instabilities can account for the strong field intensity recorded in Allende compared to other carbonaceous chondrites.

The presence of ring and gap structures in the outer solar nebula would provide a mechanism for the formation of distinct isotopic reservoirs, which have been attributed to the formation of Jupiter (Kruijer et al., 2017). If the strong magnetic fields recorded by Allende were amplified due to the formation of Jupiter (Gressel et al., 2013), our results would provide support for the hypothesis that the CV chondrites formed in the innermost region beyond Jupiter's orbit (Desch et al., 2018).

6. Conclusion

Based on spatially resolved thermal demagnetization sequences of individual mineral assemblages, we demonstrate with high confidence that the strong, unidirectional MT magnetization in the Allende CV chondrite is carried by Fe-sulfide minerals but absent from other ferromagnetic populations. Our high-resolution thermal demagnetization of laboratory magnetizations reveals a 284 ± 6°C Curie temperature, coinciding with the 290 ± 5°C maximum unblocking temperature of the MT component. Further, our ARM, partial TRM, and PRM acquisition experiments show that the FeNi assemblages are capable of acquiring magnetization when subjected to the degree of heating and shock experienced by Allende.

Consequently, the absence of the MT magnetization in FeNi assemblages, combined with petrographic observations suggesting the Fe-sulfide and FeNi populations formed contemporaneously, requires that the MT magnetization was acquired in a non-thermal process, most likely as a CRM. In this scenario, Mn-Cr and I-Xe dating of secondary phases in Allende implies that the age of magnetization is 3.0–4.2 My after CAIs.

Such an early age for the paleomagnetic record of Allende implies that the recorded field is most likely of nebular origin due to the expected late start of a dynamo. The paleointensity of the Allende magnetization, ≥40 μT after accounting for the rotation of the CV parent body, is indicative of strong MHD instability-driven amplification of magnetic fields in the outer solar system and is much higher than those recovered from other carbonaceous chondrites of similar age. This large spread in paleointensities may support temporal or spatial magnetic field variations in the solar nebula caused by MHD instabilities or planet formation, possibly similar to ring and gap structures observed in other PPDs.

Conflict of Interest

The authors declare no conflicts of interest relevant to this study.

Data Availability Statement

All data presented here are available from the Harvard Dataverse (Fu, 2020).

Acknowledgments
The authors thank D.S. Ebel for discussions and providing the Allende sample. Part of this work was performed at the Institute for Rock Magnetism (IRM) at the University of Minnesota. The IRM is a US National multiuser facility supported through the Instrumentation and Facilities program of the National Science Foundation, Earth Sciences Division, and by funding from the University of Minnesota. This is IRM publication #2103. This work was also performed in part at the Harvard Center for Nanoscale Systems (CNS), which is supported by the National Science Foundation under NSF Award 1541959. Development of QDM capabilities supported by NSF grant PHY-1843727 enabled the completion of this work. The authors thank S. Tikoo for additional discussions and G. Kletetschka, L. Tauxe, and an anonymous reviewer for comments that improved the manuscript.

References

Acton, G., Yin, Q. Z., Verosub, K. L., Jovane, L., Roth, A., Jacobsen, B., & Ebel, D. S. (2007). Micromagnetic coercivity distributions and interactions in chondrules with implications for paleointensities of the early solar system. *Journal of Geophysical Research*, *112*. B03S90. https://doi.org/10.1029/2006JB004655

Alexander, C. M. O., Fogel, M., Yabuta, H., & Cody, G. D. (2007). The origin and evolution of chondrites recorded in the elemental and isotopic compositions of their macromolecular organic matter. *Geochimica et Cosmochimica Acta*, *71*, 4380–4403. https://doi.org/10.1016/j.gca.2007.06.052

Alt, J. C., Shanks, W. C., Bach, W., Paulick, H., Garrido, C. J., & Beaudoin, G. (2007). Hydrothermal alteration and microbial sulfate reduction in peridotite and gabbro exposed by detachment faulting at the Mid-Atlantic Ridge, 15°200N (ODP Leg 209): A sulfur and oxygen isotope study. *Geochemistry, Geophysics, Geosystems*, *8*, Q08002. https://doi.org/10.1029/2007gc001617

Andrews, S., Huang, J., Pérez, L. M., Isella, A., Dullemond, C. P., Kurtovic, N. T., et al. (2018). ALMA observations of the epoch of planet formation. *The Messenger*, *174*. https://doi.org/10.18727/0722-6691/5108

Bai, X.-N. (2015). Hall Effect Controlled Gas Dynamics in Protoplanetary Disks. II. Full 3D Simulations toward the Outer Disk. *Acta Pathologica Japonica*, *798*, 84. https://doi.org/10.1088/0004-637X/798/2/84

Bai, X.-N. (2017). Global simulations of the inner regions of protoplanetary disks with comprehensive disk microphysics. *The Astrophysical Journal*, *845*, 75. https://doi.org/10.3847/1538-4357/aa7dda

Baruteau, C., Crida, A., Paardekooper, S. J., Masset, F., Guilet, J., Bitsch, B., et al. (2014). Planet-disc interactions and early evolution of planetary systems. In *Protostars and planets VI*, (p. 667). University Arizona Press.

Bennett, C. E. G., & Graham, J. (1980). New observations on natural pyrrhotites. Part III. Thermomagnetic experiments. *American Mineralogist*, *66*, 1254–1257.

Berndt, T., Muxworthy, A. R., & Fabian, K. (2016). Does size matter? Statistical limits of paleomagnetic field reconstruction from small rock specimens. *Journal of Geophysical Research: Solid Earth*, *121*, 15–26. https://doi.org/10.1002/2015JB012441

Béthune, W., Lesur, G., & Ferreira, J. (2017). Global simulations of protoplanetary disks with net magnetic flux I Non-ideal MHD case. *Astronomy & Astrophysics*, *600*, A75. https://doi.org/10.1051/0004-6361/201630056

Bland, P. A., Collins, G. S., Davison, T. M., Abreu, N. M., Ciesla, F. J., Muxworthy, A. R., & Moore, J. (2014). Pressure–temperature evolution of primordial solar system solids during impact-induced compaction. *Nature Communications*, *5*, 5451. https://doi.org/10.1038/ncomms6451

Blum, J. D., Wasserburg, G. J., Hutcheon, I. D., Stolper, E. M., & Stolper, E. M. (1989). Origin of opaque assemblages in C3V meteorites: Implications for nebular and planetary processes. *Geochimica et Cosmochimica Acta*, *53*, 543–556. https://doi.org/10.1016/0016-7037(89)90404-3

Brearley, A. J. (2006). The action of water. In D. S. Lauretta, & H. Y. McSween (Eds.), *Meteorites and the early solar system II* (pp. 587–624). University of Arizona Press.

Bryson, J. F. J., Neufeld, J. A., & Nimmo, F. (2019). Constraints on asteroid magnetic field evolution and the radii of meteorite parent bodies from thermal modelling. *Earth and Planetary Science Letters*, *521*, 67–78. https://doi.org/10.1016/j.epsl.2019.05.046

Bryson, J. F. J., Weiss, B. P., Biersteker, J. B., King, A. J., & Russell, S. S. (2020). Constraints on the distances and timescales of solid migration in the early solar system from meteorite magnetism. *The Astrophysical Journal*, *896*, 103. https://doi.org/10.3847/1538-4357/ab91ab

Butler, R. F. (1972). Natural remanent magnetization and thermomagnetic properties of Allende meteorite. *Earth and Planetary Science Letters*, *17*, 120–128. https://doi.org/10.1016/0012-821x(72)90266-x

Carporzen, L., Weiss, B. P., Elkins-Tanton, L. T., Shuster, D. L., Ebel, D. S., & Gattacceca, J. (2011). Magnetic evidence for a partially differentiated carbonaceous chondrite parent body. *Proceedings of the National Academy of Sciences of the United States of America*, *108*, 6386–6389. https://doi.org/10.1073/pnas.1017165108

Cournede, C., Gattacceca, J., Gounelle, M., Rochette, P., Weiss, B. P., & Zanda, B. (2015). An early solar system magnetic field recorded in CM chondrites. *Earth and Planetary Science Letters*, *410*, 62–74. https://doi.org/10.1016/j.epsl.2014.11.019

Crawford, D. A., & Schultz, P. H. (1988). Laboratory observations of impact-generated magnetic fields. *Nature*, *336*, 50–52. https://doi.org/10.1038/336050a0

Crawford, D. A., & Schultz, P. H. (1999). Electromagnetic properties of impact-generated plasma, vapor and debris. *International Journal of Impact Engineering*, *23*, 169–180. https://doi.org/10.1016/s0734-743x(99)00070-6

Cuvillier, P., Leroux, H., Jacob, D., & Hirel, P. (2015). Fe-Mg interdiffusion profiles in rimmed forsterite grains in the Allende matrix: Time–temperature constraints for the parent body metamorphism. *Meteoritics & Planetary Science*, *50*, 1529–1545. https://doi.org/10.1111/maps.12493

de Pater, I., & Lissauer, J. J. (2010). Chapter 3: Solar heating and energy transport, In *Planetary Sciences*. Cambridge University Press.

Desch, S. J., Kalyaan, A., & Alexander, C. M. O. (2018). The effect of Jupiter's formation on the distribution of refractory elements and inclusions in meteorites. *The Astrophysical Journal Supplement Series*, *238*, 11. https://doi.org/10.3847/1538-4365/aad95f

Dipierro, G., Laibe, G., Price, D. J., & Lodato, G. (2016). Two mechanisms for dust gap opening in protoplanetary discs. *Monthly Notices of the Royal Astronomical Society: Letters*, *459*, L1–L5. https://doi.org/10.1093/mnrasl/slw032

Dodds, K. H., Bryson, J. F. J., Neufeld, J. A., & Harrison, R. J. (2021). The thermal evolution of planetesimals during accretion and differentiation: Consequences for dynamo generation by thermally-driven convection. *Journal of Geophysical Research: Planets*, *126*, e2020JE006704. https://doi.org/10.1029/2020je006704

Doyle, P. M., Jogo, K., Nagashima, K., Krot, A. N., Wakita, S., Ciesla, F. J., & Hutcheon, I. D. (2015). Early aqueous activity on the ordinary and carbonaceous chondrite parent bodies recorded by fayalite. *Nature Communications*, *6*, 7444. https://doi.org/10.1038/ncomms8444

Dyl, K. A., Bischoff, A., Ziegler, K., Young, E. D., Wimmer, K., & Bland, P. A. (2012). Early Solar System hydrothermal activity in chondritic asteroids on 1–10-year timescales. *Proceedings of the National Academy of Sciences of the United States of America*, *109*, 18306–18311. https://doi.org/10.1073/pnas.1207475109

Emmerton, S., Muxworthy, A. R., Hezel, D. C., & Bland, P. A. (2011). Magnetic characteristics of CV chondrules with paleointensity implications. *Journal of Geophysical Research*, *116*, E12007. https://doi.org/10.1029/2011je003856

Fu, R. R. (2020). *Replication Data for: The fine-scale magnetic history of the Allende meteorite: Implications for the structure of the solar nebula*. https://doi.org/10.7910/DVN/HP3YJW

Fu, R. R., Kehayias, P., Weiss, B. P., Schrader, D. L., Bai, X.-N., & Simon, J. B. (2020). Weak magnetic fields in the outer solar nebula recorded in CR chondrites. *Journal of Geophysical Research: Planets*, *125*, e2019JE006260. https://doi.org/10.1029/2019je006260

Fu, R. R., Lima, E. A., Volk, M. W. R., & Trubko, R. (2020). High sensitivity moment magnetometry with the quantum diamond microscope. *Geochemistry, Geophysics, Geosystems*, *21*, e2020GC009147. https://doi.org/10.1029/2020gc009147

Fu, R. R., Lima, E. A., & Weiss, B. P. (2014). No nebular magnetization in the Allende CV carbonaceous chondrite: Earth Planet. *Science Letter*, *404*, 54–66. https://doi.org/10.1016/j.epsl.2014.07.014

Fu, R. R., Weiss, B. P., Lima, E. A., Harrison, R. J., Bai, X.-N., Desch, S. J., et al. (2014). Solar nebula magnetic fields recorded in the Semarkona meteorite. *Science*, *346*, 1089–1092. https://doi.org/10.1126/science.1258022

Ganino, C., & Libourel, G. (2017). Reduced and unstratified crust in CV chondrite parent body. *Nature Communications*, *8*, 261. https://doi.org/10.1038/s41467-017-00293-1

Ganino, C., & Libourel, G. (2020). Fumarolic-like activity on carbonaceous chondrite parent body. *Science Advances*, *6*, eabb1166. https://doi.org/10.1126/sciadv.abb1166

Garming, J. F. L., von Dobeneck, T., Franke, C., & Bleil, U. (2007). Low-temperature partial magnetic self-reversal in marine sediments by magnetostatic interaction of titanomagnetite and titanohematite intergrowths. *Geophysical Journal International*, *170*, 1067–1075. https://doi.org/10.1111/j.1365-246x.2007.03504.x

Gattacceca, J., Berthe, L., Boustie, M., Vadeboin, F., Rochette, P., & De Resseguier, T. (2008). On the efficiency of shock magnetization processes. *Physics of the Earth and Planetary Interiors*, *166*, 1–10. https://doi.org/10.1016/j.pepi.2007.09.005

Gattacceca, J., Boustie, M., Lima, E., Weiss, B. P., de Resseguier, T., & Cuq-Lelandais, J. P. (2010). Unraveling the simultaneous shock magnetization and demagnetization of rocks. *Physics of the Earth and Planetary Interiors*, *182*, 42–49. https://doi.org/10.1016/j.pepi.2010.06.009

Gattacceca, J., Weiss, B. P., & Gounelle, M. (2016). New constraints on the magnetic history of the CV parent body and the solar nebula from the Kaba meteorite. *Earth and Planetary Science Letters*, *455*, 166–175. https://doi.org/10.1016/j.epsl.2016.09.008

Gilmour, J. D., Crowther, S. A., Busfield, A., Holland, G., & Whitby, J. A. (2009). An early I-Xe age for CB chondrite chondrule formation, and a re-evaluation of the closure age of Shallowater enstatite. *Meteoritics & Planetary Science*, *44*, 573–579. https://doi.org/10.1111/j.1945-5100.2009.tb00752.x

Glavin, D. P., Kubny, A., Jagoutz, E., & Lugmair, G. W. (2004). Mn-Cr isotope systematics of the D'Orbigny angrite. *Meteoritics & Planetary Science*, *39*, 693–700. https://doi.org/10.1111/j.1945-5100.2004.tb00112.x

Glenn, D. R., Fu, R. R., Kehayias, P., Le Sage, D., Lima, E. A., Weiss, B. P., & Walsworth, R. L. (2017). Micrometer-scale magnetic imaging of geological samples using a quantum diamond microscope. *Geochemistry, Geophysics, Geosystems*, *18*, 3254–3267. https://doi.org/10.1002/2017GC006946

Gressel, O., Nelson, R. P., Turner, N. J., & Ziegler, U. (2013). Global hydromagnetic simulations of a planet embedded in a dead zone: Gap opening, gas accretion, and the formation of protoplanetary jet. *The Astrophysical Journal*, *779*, 59. https://doi.org/10.1088/0004-637x/779/1/59

Haggerty, S. E., & McMahon, B. M. (1979). Magnetite-sulfide-metal complexes in the Allende meteorite. *Planetary Science Conference Proceedings*, 851–870.

Haines, C. R. S., Howard, C. J., Harrison, R. J., & Carpenter, M. A. (2019). Group-theoretical analysis of structural instability, vacancy ordering and magnetic transitions in the system troilite (FeS)–pyrrhotite (Fe1-xS). *Acta Crystallographica*, *B75*, 1208–1224. https://doi.org/10.1107/s2052520619014197

Heider, F., & Dunlop, D. J. (1987). Two types of chemical remanent magnetization during the oxidation of magnetite. *Physics of the Earth and Planetary Interiors*, *46*, 24–45. https://doi.org/10.1016/0031-9201(87)90169-5

Hood, L. L., & Artemieva, N. A. (2008). Antipodal effects of lunar basin-forming impacts: Initial 3D simulations and comparisons with observations. *Icarus*, *193*, 485–502. https://doi.org/10.1016/j.icarus.2007.08.023

Horng, C.-S. (2018). Unusual magnetic properties of sedimentary pyrrhotite in methane seepage sediments: Comparison with metamorphic pyrrhotite and sedimentary greigite. *Journal of Geophysical Research: Solid Earth*, *123*. https://doi.org/10.1002/2017jb015262

Horng, C.-S., & Roberts, A. P. (2018). The low-temperature Besnus magnetic transition: Signals due to monoclinic and hexagonal pyrrhotite. *Geochemistry, Geophysics, Geosystems*, *19*, 3364–3375. https://doi.org/10.1029/2017gc007394

Hutcheon, I. D., Krot, A. N., Keil, K., Phinney, D. L., & Scott, E. R. D. (1998). 53Mn-53Cr dating of fayalite formation in CV3 chondrite Mokoia: Evidence for asteroidal alteration. *Science*, *282*, 1865–1867. https://doi.org/10.1126/science.282.5395.1865

Johansen, A. (2009). The role of magnetic fields for planetary formation. In K. G. Strassmeier, A. G. Kosovichev, & J. E. Beckman (Eds.), *Cosmic Magnetic Fields: From Planets, to Stars and Galaxies, Proceedings of IAU Symposium.* (pp. 119–128).

Johnson, B. C., Walsh, K. J., Minton, D. A., Krot, A. N., & Levison, H. F. (2016). Timing of the formation and migration of giant planets as constrained by CB chondrites. *Science Advances*, *2*, e1601658. https://doi.org/10.1126/sciadv.1601658

Kissin, S. A., & Scott, S. D. (1982). Phase relations involing pyrrhotite below 350°C. *Economic Geology*, *77*, 1739–1754. https://doi.org/10.2113/gsecongeo.77.7.1739

Klahr, H., Pfeil, T., & Schreiber, A. (2018). Instabilities and flow structures in protoplanetary disks: Setting the stage for planetesimal formation. In *Handbook of exoplanets*, (pp. 1–36). Springer. https://doi.org/10.1007/978-3-319-30648-3_138-1

Klein, F., & Bach, W. (2009). Fe-Ni-Co-O-S Phase Relations in Peridotite^Seawater Interactions. *Journal of Petrology*, *50*, 37–59. https://doi.org/10.1093/petrology/egn071

Kletetschka, G. (2018). Magnetization of Extraterrestrial Allende material may relate to terrestrial descend: Earth Planet. *Science Letter*, *487*, 1–8. https://doi.org/10.1016/j.epsl.2018.01.020

Kletetschka, G., Acuna, M. H., Kohout, T., Wasilewski, P. J., & Connerney, J. E. P. (2004). An empirical scaling law for acquisition of thermoremanent magnetization. *Earth and Planetary Science Letters*, *226*, 521–528. https://doi.org/10.1016/j.epsl.2004.08.001

Kletetschka, G., & Wieczorek, M. A. (2017). Fundamental relations of mineral specific magnetic carriers for paleointensity determination. *Physics of the Earth and Planetary Interiors*, *272*, 44–49. https://doi.org/10.1016/j.pepi.2017.09.008

Krapp, L., Gressel, O., Benítez-Llambay, P., Downes, T. P., Mohandas, G., & Pessah, M. E. (2018). Dust segregation in Hall-dominated turbulent protoplanetary disks: Astrophys. *D-J Series*, *865*, 105. https://doi.org/10.3847/1538-4357/aadcf0

Krot, A. N., Hutcheon, I. D., Brearley, A. J., Pravdivtseva, O. V., Petaev, M. I., & Hohenberg, C. M. (2006). Timescales and settings for alteration of chondritic meteorites. In D. S. Lauretta, & H. Y. McSween (Eds.), *Meteorites and the early solar system II* (pp. 525–553). University of Arizona Press.

Krot, A. N., Petaev, M. I., & Bland, P. A. (2004). Multiple formation mechanisms of ferrous olivine in CV carbonaceous chondrites during fluid-assisted metamorphism. *Antarctic Meteorite Research*, *17*, 153–171.

Krot, A. N., Petaev, M. I., Scott, E. R. D., Choi, B.-G., Zolensky, M. E., & Keil, K. (1998). Progressive alteration in CV3 chondrites: More evidence for asteroidal alteration. *Meteoritics & Planetary Science*, *33*, 1065–1085. https://doi.org/10.1111/j.1945-5100.1998.tb01713.x

Kruijer, T. S., Burkhardt, G., Budde, G., & Kleine, T. (2017). Age of Jupiter inferred from the distinct genetics and formation times of meteorites. *Proceedings of the National Academy of Sciences of the United States of America*, *14*, 6712. https://doi.org/10.1073/pnas.1704461114

Lesur, G. (2021). Magnetohydrodynamics of protoplanetary discs. *Journal of Plasma Physics*, *87*, 205870101. https://doi.org/10.1017/s0022377820001002

Lowell, R. P., & Germanovich, L. N. (1994). On the temporal evolutionof high-temperaturehydrothermal systemsat oceanridge crests. *Journal of Geophysical Research*, *99*, 565–575. https://doi.org/10.1029/93jb02568

MacPherson, G. J., & Krot, A. N. (2014). The formation of Ca-, Fe-rich silicates in reduced and oxidized CV chondrites: The roles of impact-modified porosity and permeability, and heterogeneous distribution of water ices. *Meteoritics & Planetary Science*, *49*, 1250–1270. https://doi.org/10.1111/maps.12316

MacPherson, G. J., Nagashima, K., Krot, A. N., Doyle, P. M., & Ivanova, M. A. (2017). 53Mn–53Cr chronology of Ca–Fe silicates in CV3 chondrites. *Geochimica et Cosmochimica Acta*, *201*, 260–274. https://doi.org/10.1016/j.gca.2016.09.032

McClelland, E. (1996). Theory of CRM acquired by grain growth, and its implications for TRM discrimination and palaeointensity determination in igneous rocks. *Geophysical Journal International*, *126*, 271–280. https://doi.org/10.1111/j.1365-246x.1996.tb05285.x

McClelland, E., & Goss, C. (1993). Self reversal of chemical remanent magnetization on the transformation of maghemite to haematite. *Geophysical Journal International*, *112*, 517–532. https://doi.org/10.1111/j.1365-246x.1993.tb01185.x

Min, M., Dullemond, C. P., Kama, M., & Dominik, C. (2011). The thermal structure and the location of the snow line in the protosolar nebula: Axisymmetric models with full 3-D radiative transfer. *Icarus*, *212*, 416–426. https://doi.org/10.1016/j.icarus.2010.12.002

Muxworthy, A. R., Bland, P. A., Davison, T. M., Moore, J., Collins, G. S., & Ciesla, F. J. (2017). Evidence for an impact-induced magnetic fabric in Allende, and exogenous alternatives to the core dynamo theory for Allende magnetization. *Meteoritics & Planetary Sciences*, 1–15.

Nagata, T., & Funaki, M. (1983). Paleomagnetic re-examination of the Allende carbonaceous chondrite. In *Lunar and Planetary Science Conference*, 14, 540–541.

Neumann, W., Breuer, D., & Spohn, T. (2014). Differentiation of Vesta: Implications for a shallow magma ocean. *Earth and Planetary Science Letters*, *395*, 267–280. https://doi.org/10.1016/j.epsl.2014.03.033

O'Brien, T., Tarduno, J. A., Anand, A., Smirnov, A. V., Blackman, E. G., Carroll-Nellenback, J., & Krot, A. N. (2020). Arrival and magnetization of carbonaceous chondrites in the asteroid belt before 4562 million years ago. *Communications Earth & Environment*, *1*, 54.

Ohnaka, M., & Kinoshita, H. (1968). Effects of uniaxial compression on remanent magnetization. *Journal of Geomagnetism and Geoelectricity*, *20*, 93–99. https://doi.org/10.5636/jgg.20.93

Oran, R., Weiss, B. P., & Cohen, O. (2018). Were chondrites magnetized by the early solar wind? *Earth and Planetary Science Letters*, *492*, 222–231. https://doi.org/10.1016/j.epsl.2018.02.013

Özdemir, Ö., & Dunlop, D. J. (1985). An experimental study of chemical remanent magnetizations of synthetic monodomain titanomaghemites with initial thermoremanent magnetizations. *Journal of Geophysical Research*, *90*(11), 513–611. https://doi.org/10.1029/jb090ib13p11513

Partnership, A. L. M. A., Brogan, C. L., Pérez, L. M., Hunter, T. R., Dent, W. R. F., Hales, A. S., et al. (2015). The 2014 ALMA long baseline campaign: First results from high angular resolution observations toward the HL Tau region. *The Astrophysical Journal Letters*, *808*, L3. https://doi.org/10.1088/2041-8205/808/1/l3

Pravdivtseva, O., Meshik, A., & Hohenberg, C. M. (2013). *The I-Xe record: Early onset of aqueous alteration in magnetites separated from CM and CV carbonaceous chondrites*.

Pravdivtseva, O. V., Krot, A. N., Hohenberg, C. M., Meshik, A. P., Weisberg, M., & Keil, K. (2003). The I-Xe record of alteration in the Allende CV chondrite. *Geochimica et Cosmochimica Acta*, *67*, 5011–5026. https://doi.org/10.1016/s0016-7037(03)00274-6

Riols, A., & Lesur, G. (2019). Spontaneous ring formation in wind-emitting accretion discs. *Astronomy & Astrophysics*, *625*, A108. https://doi.org/10.1051/0004-6361/201834813

Riols, A., Lesur, G., & Menard, F. (2020). Ring formation and dust dynamics in wind-driven protoplanetary discs: Global simulationss. *Astronomy & Astrophysics*, *639*, A95. https://doi.org/10.1051/0004-6361/201937418

Roberts, A. P., & Turner, G. M. (1993). Diagenetic formation of ferrimagnetic iron sulphide minerals in rapidly deposited marine sediments, South Island, New Zealand. *Earth and Planetary Science Letters*, *115*, 257–273. https://doi.org/10.1016/0012-821x(93)90226-y

Rochette, P., Fillion, G., Ballou, R., Brunet, F., Ouladdiaf, B., & Hood, L. (2003). High pressure magnetic transition in pyrrhotite and impact demagnetization on Mars. *Geophysical Research Letters*, *30*, 1683. https://doi.org/10.1029/2003gl017359

Rochette, P., Lorand, J. P., Fillion, G., & Sautter, V. (2001). Pyrrhotite and the remanent magnetization of SNC meteorites: A changing perspective on Martian magnetism. *Earth and Planetary Science Letters*, *190*, 1–12. https://doi.org/10.1016/s0012-821x(01)00373-9

Schrader, D. L., Nagashima, K., Krot, A. N., Ogliore, R. C., Yin, Q. Z., Amelin, Y., et al. (2017). Distribution of 26Al in the CR chondrite chondrule-forming region of the protoplanetary disk. *Geochimica et Cosmochimica Acta*, *201*, 275–302. https://doi.org/10.1016/j.gca.2016.06.023

Shu, F. H., Shang, H., Glassgold, A. E., & Lee, T. (1997). X-rays and fluctuating x-winds from protostars. *Science*, *277*, 1475–1479. https://doi.org/10.1126/science.277.5331.1475

Stokking, L. B., & Tauxe, L. (1990). Propertites of chemical remanence in synthetic hematite: Testing theoretical predictions. *Journal of Geophysical Research*, *95*(12), 612–639. https://doi.org/10.1029/jb095ib08p12639

Sugiura, N., Lanoix, M., & Strangway, D. W. (1979). Magnetic fields of the solar nebula as recorded in chondrules from the Allende meteorite. *Physics of the Earth and Planetary Interiors*, *20*, 342–349. https://doi.org/10.1016/0031-9201(79)90056-6

Sugiura, N., & Strangway, D. W. (1985). NRM directions around a centimeter-sized dark inclusion in Allende.In *Proceedings of Planetary Science Conference 15th* (pp. C729–C738). https://doi.org/10.1029/jb090is02p0c729

Suriano, S. S., Li, Z.-Y., Krasnopolsky, R., & Shang, H. (2018). The formation of rings and gaps in magnetically coupled disc-wind systems: Ambipolar diffusion and reconnection. *Monthly Notices of the Royal Astronomical Society*, *477*, 1239–1257. https://doi.org/10.1093/mnras/sty717

Sutton, S., Alexander, C. M. O., Bryant, A., Lanzirotti, A., Newville, M., & Cloutis, E. A. (2017). The bulk valence state of Fe and the origin of water in chondrites. *Geochimica et Cosmochimica Acta*, *211*, 115–132. https://doi.org/10.1016/j.gca.2017.05.021

Swindle, T. D., Caffee, M. W., Hohenberg, C. M., & Lindstrom, M. M. (1983). I-Xe studies of individual Allende chondrules. *Geochimica et Cosmochimica Acta*, *47*, 2157–2177. https://doi.org/10.1016/0016-7037(83)90040-6

Tarduno, J. A., O'Brien, T. M., Anand, A., Blackman, E. G., Smirnov, A. V., & Carroll-Nellenback, J. (2020). *External magnetization of carbonaceous chondrites at 2-4 AU, 4.2-48 million years of CAI formation* (p. 2676). Houston, TX. USRA.

Volk, M. W. R., & Gilder, S. A. (2016). Effect of static pressure on absolute paleointensity recording with implications for meteorites. *Journal of Geophysical Research: Solid Earth*, *121*, 5596–5610. https://doi.org/10.1002/2016jb013059

Wang, H., Weiss, B. P., Bai, X.-N., Downey, B. G., Wang, J., Wang, J., et al. (2017). Lifetime of the solar nebula constrained by meteorite paleomagnetism. *Science*, *355*, 623–627. https://doi.org/10.1126/science.aaf5043

Wasilewski, P. (1981). New magnetic results from Allende C3(V). *Physics of the Earth and Planetary Interiors*, *26*, 134–148. https://doi.org/10.1016/0031-9201(81)90105-9

Wasilewski, P. J., & Saralker, C. (1981). Stable NRM and mineralogy in Allende: Chondrules. In *Lunar and Planetary Science Conference 12th*, 1217–1227

Watson, G. S. (1956). A test for randomness. *Monthly Notices of the Royal Astronomical Society*, *7*, 160–161. https://doi.org/10.1111/j.1365-246x.1956.tb05561.x

Weaver, R., Roberts, A. P., & Barker, A. J. (2002). A late diagenetic (syn-folding) magnetization carried by pyrrhotite: Implications for paleomagnetic studies from magnetic iron sulphide-bearing sediments. *Earth and Planetary Science Letters*, *200*, 371–386. https://doi.org/10.1016/s0012-821x(02)00652-0

Weiss, B. P., Bai, X.-N., & Fu, R. R. (2021). History of the solar nebula from meteorite paleomagnetism. *Science Advances*, *7*, eaba5967. https://doi.org/10.1126/sciadv.aba5967

Weiss, B. P., Gattacceca, J., Stanley, S., Rochette, P., & Christensen, U. R. (2010). Paleomagnetic records of meteorites and early planetesimal differentiation. *Space Science Reviews*, *152*, 341–390. https://doi.org/10.1007/s11214-009-9580-z

Weiss, B. P., Lima, E. A., & Zucolotto, M. E. (2008). Magnetism on the angrite parent body. *Lunar and Planetary Science*, *39*. https://doi.org/10.1002/chin.200842270

Xu, W., Van der Voo, R., & Peacor, D. R. (1998). Electron microscopic and rock magnetic study of remagnetized Leadville carbonates central Colorado. *Tectonophysics*, *296*, 333–362. https://doi.org/10.1016/s0040-1951(98)00146-2

Zegers, T. E., Dekkers, M. J., & Bailly, S. (2003). Late Carboniferous to Permian remagnetization of Devonian limestones in the Ardennes: Role of temperature, fluids, and deformation. *Journal of Geophysical Research*, *108*, 2357. https://doi.org/10.1029/2002jb002213